

Split Ga vacancies and the colossal anisotropy of positron annihilation spectra in $\beta\text{-Ga}_2\text{O}_3$

Antti Karjalainen,^{1, 2} Vera Prozheeva,² Kristoffer Simula,¹ Ilja Makkonen,^{1, 2, 3}
Vincent Callewaert,⁴ Joel B. Varley,⁵ and Filip Tuomisto^{1, 2, 3}

¹*Department of Physics, University of Helsinki, P.O. Box 43, FI-00014 Helsinki, Finland*

²*Department of Applied Physics, Aalto University, P.O. Box 15100, FI-00076 Espoo, Finland*

³*Helsinki Institute of Physics, P.O. Box 64, FI-00014 Helsinki, Finland*

⁴*Department of Physics, Universiteit Antwerpen, Antwerpen 2020, Belgium*

⁵*Lawrence Livermore National Laboratory, Livermore, CA 94550, USA*

(Dated: June 18, 2022)

We report a systematic first principles study on positron annihilation parameters in the $\beta\text{-Ga}_2\text{O}_3$ lattice and Ga mono-vacancy defects complemented with direction-dependent experiments of the Doppler broadening of the positron-electron annihilation. We find that both the $\beta\text{-Ga}_2\text{O}_3$ lattice and the considered defects exhibit colossal anisotropy in their Doppler broadening signals. This anisotropy is associated with the unusual kind of low symmetry of the $\beta\text{-Ga}_2\text{O}_3$ crystal structure that leads to one-dimensional confinement of positrons even in the delocalized state in the lattice. In particular, the split Ga vacancies recently observed by scanning transmission electron microscopy produce unusually anisotropic positron annihilation signals. We show that in experiments, the positron annihilation signals in $\beta\text{-Ga}_2\text{O}_3$ samples are dominated by split Ga vacancies.

I. INTRODUCTION

$\beta\text{-Ga}_2\text{O}_3$ is a direct wide bandgap (4.9 eV) semiconductor material with a high break-down electric field of 8 MV cm⁻¹ and whose properties surpass those of GaN and SiC from the point of view of UV and high power applications [1]. As the already better characteristics are combined with the economical advantage of the availability of large size bulk crystals, $\beta\text{-Ga}_2\text{O}_3$ has earned a substantial research interest. The research efforts have led to controllable *n*-type conductivity via doping with Sn, Si or Ge [1] and unipolar field effect transistors and Schottky diodes have been developed [2].

The rapid refinement of synthesis approaches of both epitaxial and bulk $\beta\text{-Ga}_2\text{O}_3$ has led to the situation where the crystalline quality of the material is no longer the main concern. Instead, recent reviews on $\beta\text{-Ga}_2\text{O}_3$ point out that the identification and control of dominating (point and extended) defects is the most important step for further improvement of the properties of $\beta\text{-Ga}_2\text{O}_3$ devices [1, 3]. The low symmetry of the $\beta\text{-Ga}_2\text{O}_3$ structure is accompanied with anisotropic thermal, electrical and optical properties [4, 5]. Theoretical work suggested already early on that the mono-vacancy defect of the lowest formation energy in $\beta\text{-Ga}_2\text{O}_3$ is of a peculiar type [6], where a cation atom neighbouring the cation mono-vacancy relaxes to an interstitial site half-way towards the vacancy [7, 8]. These “split” Ga vacancies in which the open volume is split into two parts on either side of the interstitial, have been recently experimentally observed in infrared spectroscopy (hydrogenated form) and scanning transmission electron microscopy (STEM) studies [9, 10].

Positron annihilation spectroscopy is a non-destructive method with selective sensitivity to neutral and negative vacancy-type defects, and second-order sensitivity

to negatively charged defects without open volume [11]. Thanks to these properties, positron annihilation methods have been successful in identifying the role of native point defects in the electrical compensation of *n*-type doped compound semiconductors such as GaN, ZnO, AlN, InN and In₂O₃ [12–16], as well as their alloys such as InGaN and AlGaN [17–22]. In spite of the otherwise significant research interest in $\beta\text{-Ga}_2\text{O}_3$, the number of reported studies with positron annihilation is surprisingly low [23–25]. These studies suggest that cation vacancies contribute to the compensation of *n*-type conductivity, but also point out a potential difficulty in interpreting the positron annihilation signals.

In this work, we address the primary difficulty in studying defects with positron annihilation in $\beta\text{-Ga}_2\text{O}_3$, manifested by a colossal anisotropy of measured Doppler broadening signals. We present a comprehensive study of positron annihilation signals in $\beta\text{-Ga}_2\text{O}_3$, made possible by recent developments in theoretical calculation schemes. We show that the Doppler broadening signals emitted from positron-electron annihilations in $\beta\text{-Ga}_2\text{O}_3$ are characterized by an anisotropy of unprecedented magnitude for 3D crystals, and by relatively small differences between signals originating from the perfect lattice and various types of vacancy defects. Together, these effects cause the lattice and vacancy signals to overlap in a way that makes defect identification impossible if exact sample orientations are not determined in the experiments. A further complication arises from the lack of suitable reference $\beta\text{-Ga}_2\text{O}_3$ material where the positron annihilation data could be interpreted as originating from the lattice only, typically referred to as “defect-free reference”. Finally, by comparing to experiments, we show that the colossal signal anisotropy – in particular the differences in the nature of the anisotropy – contains information that can be used for defect identification. We provide evidence of the experimental positron annihila-

tion signals being dominated by the split Ga vacancies, supporting the recent findings [6, 7, 9, 10]. It is likely that different levels of hydrogenation of these split Ga vacancies determine the level of electrical compensation in *n*-type β -Ga₂O₃.

The remainder of this paper is organized as follows. Section II gives a brief account of the modeling scheme. In Section III, we calculate the positron annihilation signals in the β -Ga₂O₃ lattice and compare the observed anisotropy to that in other semiconductor crystals. Section IV presents the results obtained in 9 different vacancy defects, demonstrating the increase in anisotropy of the signals and full overlap with the lattice signals. In Section V we compare the calculated signal anisotropies to those found in experiments, to find that the experimental signals are most likely dominated by the split Ga vacancy effects. The discussion in Section VI is divided into two parts: in VI A we discuss the implications of our findings on defect identification in β -Ga₂O₃ and in VI B we discuss the physical origin of the observed anisotropy in the positron annihilation signals. We summarize our paper in Section VII. The Appendix provides the calculated ratio curves in all major lattice directions as well as (*S*, *W*) plots with alternative parametrization for the benefit of future defect identification endeavours.

II. MODELING POSITRON STATES AND ANNIHILATION IN β -Ga₂O₃

We study the β -Ga₂O₃ lattice and its defects using density-functional calculations and the Heyd-Scuseria-Ernzerhof (HSE06) screened hybrid functional with a modified fraction of Hartree-Fock exchange of 35% consistent with earlier work [6], and include the semi-core Ga 3d electrons as explicit valence states. We use monoclinic 160-atom supercells to describe the previously considered defect models [6, 7]. We apply the VASP code [26–28] and its implementation of the projector augmented-wave (PAW) method [29].

We model delocalized and trapped positrons and their lifetimes using the two-component density functional theory for electron-positron systems and approximating the correlation potential and enhancement factor using the local density approximation [30]. We assume that the localized positron does not affect the average electron density and apply the zero-positron-density limits of the functionals. This method, which is justified for delocalized positrons, has been shown to give also for localized positrons results that are in agreement with more self-consistent modeling [31]. We model the momentum densities of annihilating electron-positron pairs using the model by Alatalo and coworkers [32], a $2 \times 2 \times 2$ Γ -centered mesh and reconstructed PAW wave functions [33]. In order to be able to compare with Doppler broadening experiments, the 3-dimensional momentum density $\rho(\mathbf{p})$ is first projected into the desired crystal direction (as illus-

trated in Fig. 1) to give the Doppler spectrum,

$$\rho(p_L) = \int \int \rho(\mathbf{p}) dp_x dp_y, \quad (1)$$

which is then convoluted with the experimental resolution function (a Gaussian with a full width at half maximum corresponding to 0.95 keV or 1.25 keV, in case of two-detector coincidence and one-detector measurements used to obtain the shape parameters (*S*, *W*), respectively.) In order to be able to consider the monoclinic cell and projections to any lattice direction (arbitrary \mathbf{p}_L), we have implemented in our code the tetrahedron projection algorithm of Matsumoto, Tokii and Wakoh [34].

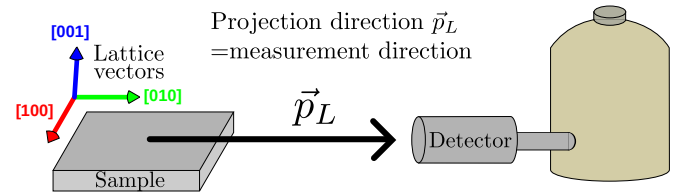


FIG. 1: Illustration of the projection direction \mathbf{p}_L with respect to the experiment geometry.

III. POSITRONS IN THE β -Ga₂O₃ LATTICE

β -Ga₂O₃ is the most stable phase of Ga₂O₃ and it has a monoclinic crystal structure with relatively low symmetry. The primitive unit cell of β -Ga₂O₃ consists of 10 atoms but due to its difficult shape the *standard conventional* unit cell is typically used. The standard conventional unit cell is almost cubic apart from one angle of 103.7° (between the [100] and [001] lattice vectors) and consists of 20 atoms (Fig. 2a). We use the standard conventional unit cell throughout this paper, and refer to it as the *unit cell*. Due to the non-orthogonal structure, the lattice planes described by Miller indices (100) and (001) are not parallel to the planes spanned by the lattice vectors and, for the sake of simplicity, we define lattice planes by the two lattice vectors spanning the plane.

The low symmetry of the lattice is well visible in the atomic structure as the lattice appears clearly different from all three lattice vector directions (see Fig. 2). Note that the structure has open “channels” in the direction of the [010] lattice vector while the cross sections perpendicular to the [100] and [001] lattice vectors appear clearly denser. There are two inequivalent Ga atoms in β -Ga₂O₃ with 4 and 6 nearest neighbour oxygen atoms (Ga(1) and Ga(2), respectively) and three inequivalent oxygen atoms. One of the rare symmetries β -Ga₂O₃ lattice has is a 180° rotation with the [010] lattice direction as the rotation axis. Following this symmetry, the unit cell has all these five inequivalent atoms (two Ga and three O) in two different orientations twice.

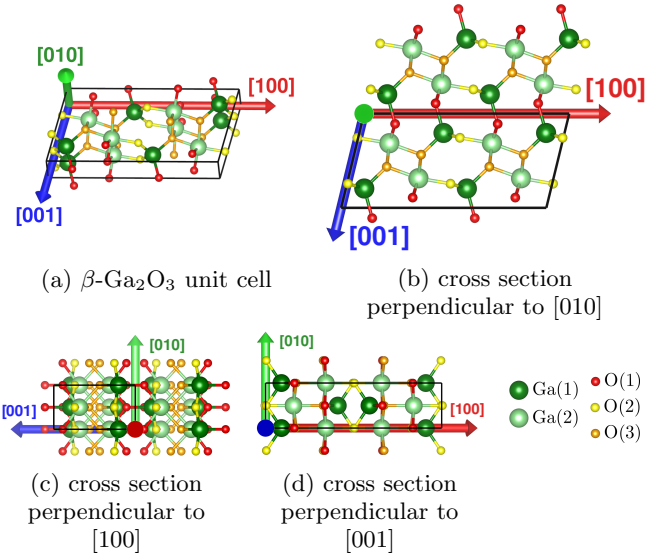


FIG. 2: The standard conventional unit cell of β - Ga_2O_3 and cross sections perpendicular to lattice vectors [35].

The positron density of the delocalized state in the β - Ga_2O_3 lattice is shown in Fig. 3 together with In_2O_3 , Si and ZnO for comparison. Interestingly, the positron density in the β - Ga_2O_3 lattice forms one-dimensional tubes along the $[010]$ lattice vector, while in the other 3D crystalline structures in Fig. 3 the positron density is rather homogeneously distributed in all three dimensions. A similar (but two-dimensional) delocalized positron state is known to exist in layered lattice structures such as graphite [38, 39], while one-dimensional positron states have been proposed to exist in carbon nanotubes [40].

Fig. 4a shows the calculated momentum distribution of annihilated electron-positron pairs (Doppler broadened spectrum) in the $[001]$ lattice direction of the β - Ga_2O_3 lattice. The calculation for the missing $\text{Ga}(1)$ atom ($\text{Ga}(1)$ vacancy), denoted by $V_{\text{Ga}1}$, is shown for comparison. Changes in the Doppler spectrum are best monitored by so-called ratio curves where the Doppler spectra are normalized by a common reference spectrum due to the differences being on the percent-level in a signal whose intensity covers several orders of magnitude. Fig. 4b shows the calculated lattice Doppler spectra in the $[100]$ and $[010]$ directions as well as the $V_{\text{Ga}1}$ spectrum in the $[001]$ direction, all normalized by the lattice spectrum in the $[001]$ direction. The anisotropy problem manifests itself immediately: the lattice spectrum in the $[010]$ direction has very similar intensity in the low momentum range (the S parameter region) as the $V_{\text{Ga}1}$ spectrum in the $[001]$ direction. In addition, the high-momentum range, even if clearly different for these two when presented as in Fig. 4a, becomes very similar upon integration due the rapidly decreasing signal intensity in the W parameter region. A detailed experimental identification would require a well-specified experimental reference spectrum that for β - Ga_2O_3 does not exist. The

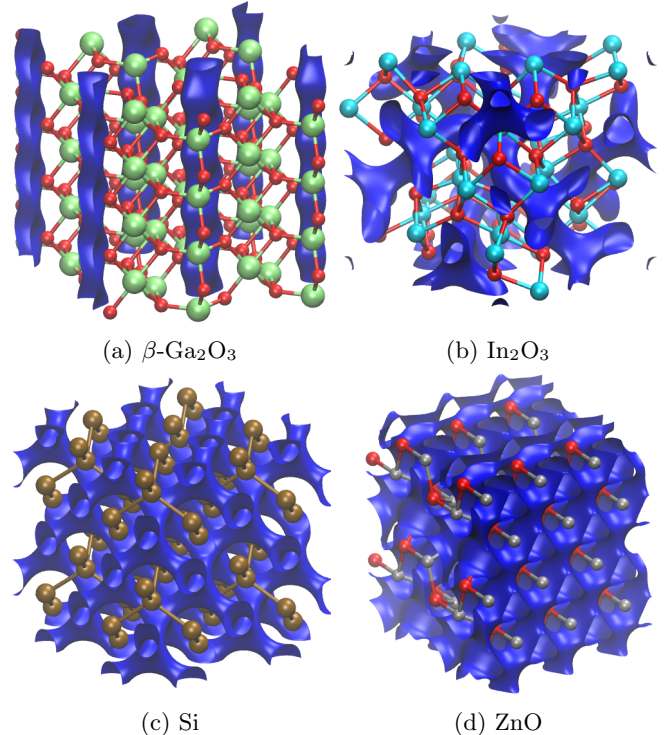


FIG. 3: Positron lattice state densities in β - Ga_2O_3 , In_2O_3 , Si and ZnO (positron density in blue, oxygen atoms in red) [36, 37]. Typically, the delocalized positron lattice state is three-dimensional but in β - Ga_2O_3 the positron density forms "tubes" along the $[010]$ lattice vector.

differences between the lattice spectra in $[001]$ and $[100]$ directions are clearly smaller.

Producing experimental ratio curves is slow due to limited count rates imposed by the coincidence detection of annihilation photons. As a consequence, the shape of the Doppler spectrum is often described with shape parameters (S, W). These parameters are defined as the fraction of annihilated electron-positron pairs in low (S) and high (W) momentum regions, shown as the shaded areas in Fig. 4. The intensity of a Doppler spectrum decreases rapidly towards higher momenta (as seen in Fig. 4a), and especially in the W parameter region the first half atomic units (a.u.) of the W window contain approximately half of the signal weight (number of counts in the experiments) of the W parameter. Note that in the ratio curves (Fig. 4b) the signal intensity is normalized to 1 and the (relative) (S, W) parameters cannot be determined by directly integrating the data in the (S, W) windows of a ratio plot.

The S parameter window is typically set in such a way that approximately half of the distribution weight (half of the counts in the experiment) is within the window (Fig. 4), to retain the statistical accuracy of collecting a large number of counts in the experiment. The lower limit of the W parameter integration window is chosen

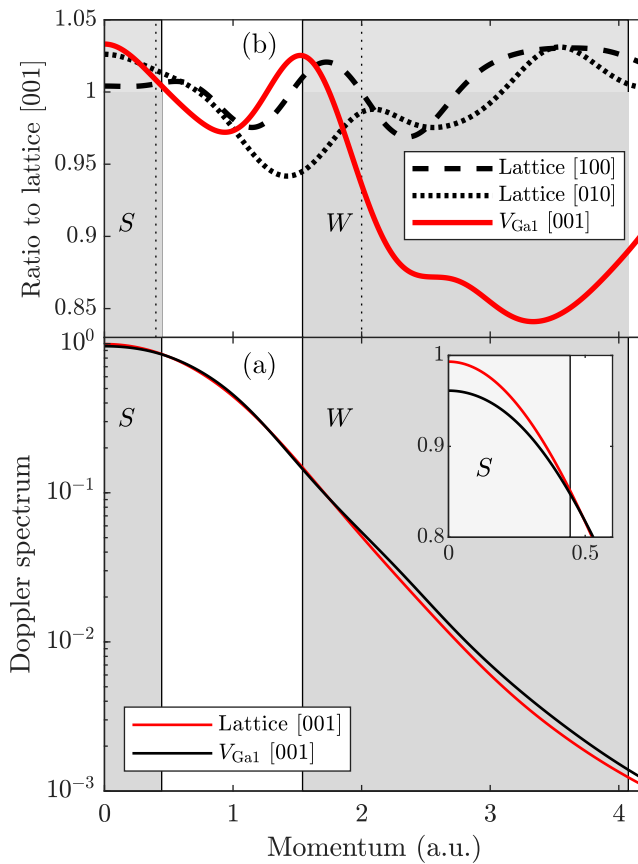
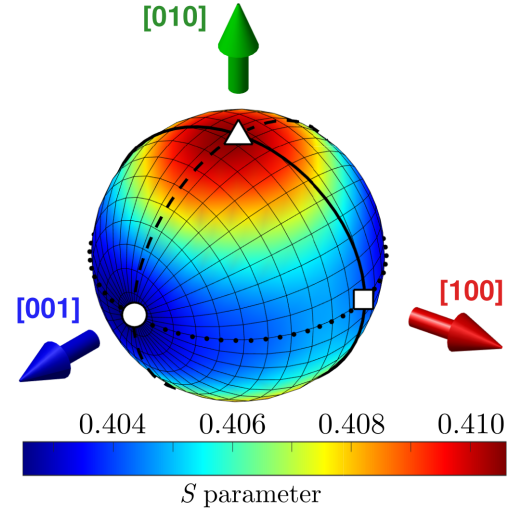


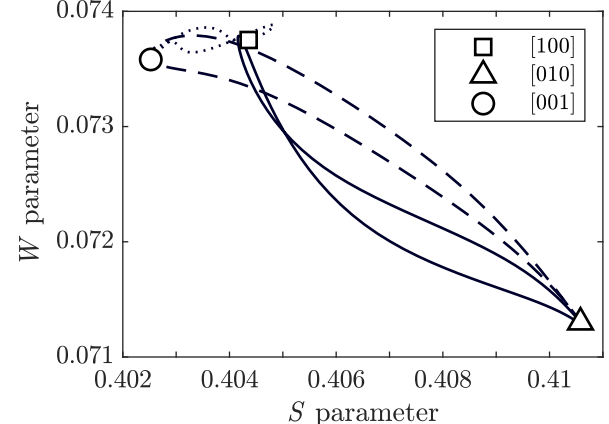
FIG. 4: (a) Calculated Doppler spectra in the β - Ga_2O_3 lattice and $V_{\text{Ga}1}$ in the [001] lattice direction. The inset shows a magnification of the S parameter region on the linear scale. (b) Ratios of the calculated Doppler spectra in the β - Ga_2O_3 lattice in the [100] and [010] lattice directions, and $V_{\text{Ga}1}$ in the [001] lattice direction, normalized by the lattice Doppler spectrum in the [001] lattice direction. The shaded regions show the integration windows of the (S, W) parameters, and the dotted vertical lines represent alternative (S, W) parameter windows.

far enough from the peak center in order to have a minimal contribution from the "free-electron" distribution that dominates the S parameter region (see Fig. 7 of Ref. 11). However, pushing the lower limit of the W parameter too far quickly deteriorates the statistical accuracy of the parameter due to the close-to-exponentially decreasing signal intensity in this range. The (S, W) parameter windows used in this work are shown in the figure with shaded areas: the S parameter window ranges from 0 to 0.45 atomic units (a.u.) and the W window from 1.54 to 4.07 a.u. The dotted lines in Fig. 4b represent alternative (S, W) windows, discussed in the Appendix. We wish to stress that while the (S, W) windows should be optimized for each material [41], in practice they often

are not and "standard" windows are used instead, and the (S, W) windows used in this work are similar to the "standard" windows. At this point we also wish to point out the fact that the (S, W) parameters only describe the shape of the Doppler spectrum, without any direct physical interpretation.



(a) Full anisotropy of the S parameter with respect to the β - Ga_2O_3 lattice vectors.



(b) The Doppler spectrum anisotropy in the (S, W) plot.

FIG. 5: Anisotropy of the Doppler signal of the β - Ga_2O_3 lattice. The full line, dashed line, and dotted curves along the geodesics between the lattice directions [001], [010] and [100] are the same in (a) and (b).

The full three-dimensional anisotropy of the S parameter in the β - Ga_2O_3 lattice is shown in Fig. 5a. The highest S parameter lies in the [010] direction ($S = 0.411$) and it decreases towards the plane spanned by the [100] and [001] lattice vectors. At angles less than 45° from the [010] lattice vector, the S parameter does not change with rotation around the [010] lattice vector. At angles higher than 45° from the [010] lattice vector the S parameters start to differ noticeably and, in the [100]-[001]

plane (90° from [010]) the S parameter is the highest in the vicinity of the [100] ($S = 0.405$) direction and the smallest in the direction of the [001] lattice vector ($S = 0.403$). While Fig. 5a may be visually appealing, comparing the full three-dimensional anisotropies in this way is not optimal. It turns out that the interesting features of the (S, W) parameters such as maxima and minima tend to be located either at the lattice vector directions or on the geodesics connecting them. Hence, we limit our discussion to these directions, as shown in Figs. 5a and 5b. The notation of Fig. 5b is used throughout the discussion: the lattice directions [100], [010] and [001] are represented by square, triangle and circle, and the geodesics between [100] and [010] are described with a full curve, between [010] and [001] with a dashed curve, and between [001] and [100] with dotted curve, as they appear on the sphere in Fig. 5a.

Figure 5b shows the (S, W) parameters in the $\beta\text{-Ga}_2\text{O}_3$ lattice. The (S, W) parameters in the [100] and [001] lattice directions are very similar, the S parameters differ by a factor of 1.005 and the W parameters are practically identical, while the [010] direction has much higher S and smaller W parameters. The extrema of the Doppler signal anisotropy are approximately at the lattice vector directions. Along the geodesics between the lattice vectors, (S, W) deviate somewhat from linear interpolation. The range of the Doppler signal anisotropy in the $\beta\text{-Ga}_2\text{O}_3$ lattice is 1.000-1.020 in the S parameter and 0.97-1.00 in the W parameter for the selected integration windows. We define the anisotropy range as the maximum and minimum S (W) parameter divided by the S (W) of the $\beta\text{-Ga}_2\text{O}_3$ lattice in the [001] lattice direction (the direction of the smallest S parameter in the $\beta\text{-Ga}_2\text{O}_3$ lattice). We use these values as the reference (S, W) point throughout the discussion.

TABLE I: Comparison of Doppler signal anisotropies in lattice and monovacancy-lattice ratios in $\beta\text{-Ga}_2\text{O}_3$, GaN and ZnO.

| Lattice anisotropy | | Vacancy/lattice-ratio | |
|-------------------------|-----------------------|------------------------------------|------------------------------------|
| $S_{[010]}/S_{[001]}$ | $W_{[010]}/W_{[001]}$ | $S_{[001]}^{\text{vac}}/S_{[001]}$ | $W_{[001]}^{\text{vac}}/W_{[001]}$ |
| Ga_2O_3 | 1.020 | 0.97 | 1.020 |
| | | | 0.96 |
| S_a/S_c | W_a/W_c | S_c^{vac}/S_c | W_c^{vac}/W_c |
| GaN | 1.003 | 0.99 | 1.071 |
| ZnO | 1.004 | 1.00 | 1.057 |
| | | | 0.82 |

It is worth noting that the Doppler broadening signals from crystal lattices are anisotropic by nature and observed in, e.g., Si [42] and ZnO [43], and that it is the magnitude of the phenomenon that is unusual and causes characterization difficulties in $\beta\text{-Ga}_2\text{O}_3$. Figure 6 shows the calculated Doppler ratio curve anisotropies and the monovacancy/lattice ratios for wurtzite GaN, wurtzite ZnO and $\beta\text{-Ga}_2\text{O}_3$. It is clearly seen that the S parameter

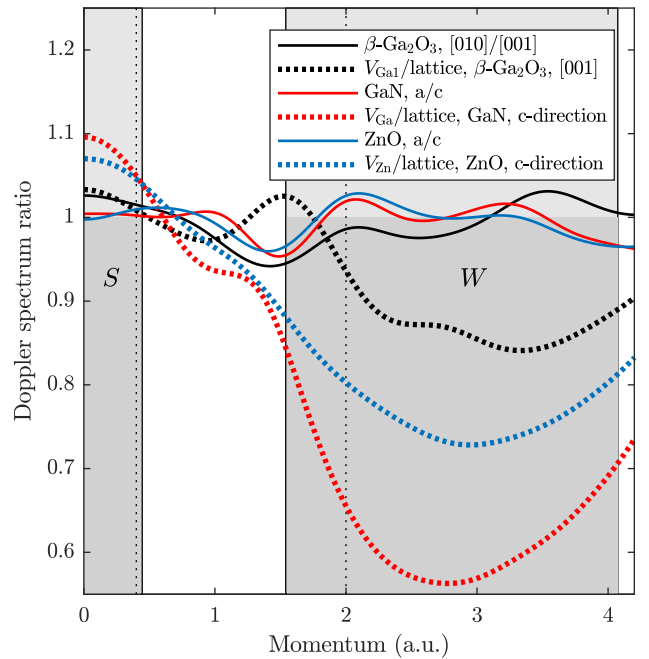


FIG. 6: Doppler signal ratios for the lattice between different projection directions as well as monovacancy-lattice ratios in $\beta\text{-Ga}_2\text{O}_3$, GaN and ZnO.

region hardly changes when examined along the a or c directions of the wurtzite lattice of GaN or ZnO, and, while the differences are larger in the W parameter region, the ratio is still very close to unity. In contrast, the monovacancy/lattice ratios are very different from the respective lattice anisotropies both for V_{Zn} in ZnO and for V_{Ga} in GaN.

Table I shows the changes in the values of the (S, W) parameters for the lattice anisotropies and the monovacancy/lattice comparisons. In GaN and ZnO, the a/c -ratios of the lattice Doppler signal are less than 1.005 in the S and 0.99 in the W parameter, and the anisotropies of the monovacancy signals in GaN and ZnO are similar or smaller. The differences between monovacancy and lattice are more than tenfold compared to the anisotropy in these two materials: the calculated monovacancy/lattice ratio in GaN is 1.071 in the S and 0.71 in the W parameter, and in ZnO they are 1.057 and 0.82, respectively. If the positron signal anisotropy is significantly smaller than the vacancy/lattice signal ratio, the anisotropy does not affect the interpretation of the experimental results in practice and can be mostly disregarded in the analysis. However, in $\beta\text{-Ga}_2\text{O}_3$, the monovacancy-lattice signal ratio is much smaller than that in GaN and ZnO, while the positron signal anisotropy in $\beta\text{-Ga}_2\text{O}_3$ is an order of magnitude stronger than in GaN or ZnO. Even in Si, where the difference between the [100] and [110] lattice directions is larger than in the wurtzite compounds [42], the anisotropy is vanishingly

small compared to that found in $\beta\text{-Ga}_2\text{O}_3$. As a result, the Doppler signal anisotropy is of the same magnitude as the monovacancy/lattice-ratio implying that $\beta\text{-Ga}_2\text{O}_3$ needs to be treated differently than other semiconductor materials.

IV. POSITRONS IN VACANCY DEFECTS OF $\beta\text{-Ga}_2\text{O}_3$

A. Structure of vacancies

In spite of $\beta\text{-Ga}_2\text{O}_3$ consisting of only two different elements, it hosts a wide variety of different monovacancy-size defects due to the inequivalent Ga and O sites. As the oxygen monovacancies were found not to trap positrons in the calculations as is usual for oxides due the small size of the open volume [44], we focus on cation monovacancies in the following. The two inequivalent Ga atoms, the four-fold coordinated Ga(1) and the six-fold coordinated Ga(2) of the $\beta\text{-Ga}_2\text{O}_3$ unit cell immediately lead to two different Ga monovacancies $V_{\text{Ga}1}$ and $V_{\text{Ga}2}$. The cation monovacancies in $\beta\text{-Ga}_2\text{O}_3$ have a special property that the regular monovacancies, $V_{\text{Ga}1}$ and $V_{\text{Ga}2}$, can relax into three different configurations $V_{\text{Ga}}^{\text{ia}}$, $V_{\text{Ga}}^{\text{ib}}$ and $V_{\text{Ga}}^{\text{ic}}$ [6, 7]. In the relaxation process, a neighbouring four-fold coordinated Ga(1) atom relaxes inwards into the interstitial space. The resulting split Ga vacancy has an open volume on both sides of the center interstitial, resulting in two "half-vacancies". The split Ga vacancy $V_{\text{Ga}}^{\text{ia}}$ forms at Ga(1) and Ga(2) sites, while $V_{\text{Ga}}^{\text{ib}}$ and $V_{\text{Ga}}^{\text{ic}}$ are formed by two Ga(1) sites, as illustrated in Fig. 7. The split Ga vacancies classify as mono-vacancies as they consist of only one missing atom.

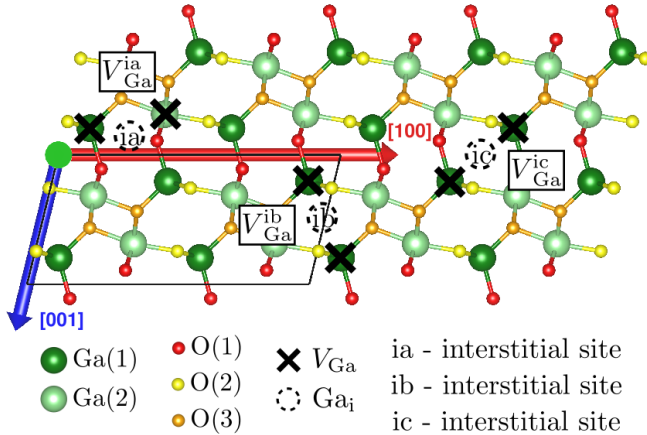


FIG. 7: The structure of split-vacancies in $\beta\text{-Ga}_2\text{O}_3$ [35].

Due to the symmetry of the $\beta\text{-Ga}_2\text{O}_3$ lattice with respect to the 180° rotation with [010] as the rotation axis, all vacancy structures in $\beta\text{-Ga}_2\text{O}_3$ appear in these two orientations. The Doppler broadening signal is intrinsically inversion symmetric, rendering the Doppler signals

of both orientations identical in the [010] lattice direction and the [100]-[001] lattice plane, but does not cancel all the differences in the directions between the [100]-[001] lattice plane and the [010] lattice direction. The presence of defects in these two orientations can be taken into account by calculating the Doppler broadening signal for one of these orientations and applying a simple correction based on symmetry. Assuming that defects appear with equal probability in both of these identical orientations, a correction for the Doppler signal, DB , can be calculated for any given direction with an angle α from [100]-[001] lattice plane (see Fig. 8). The corrected signal DB_{corr} is a mirror average with respect to the [010] lattice vector:

$$DB_{\text{corr}}(\alpha) = \frac{DB_{\text{uncorr}}(\alpha) + DB_{\text{uncorr}}(\pi - \alpha)}{2}, \quad (2)$$

where DB_{uncorr} stands for the uncorrected calculated signal.

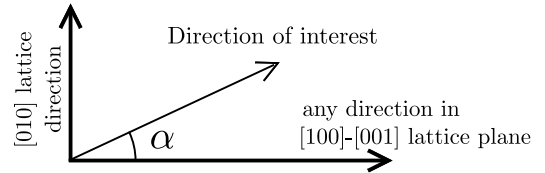


FIG. 8: Illustration of the angle α in Eq. 2 for taking account the Doppler signals of defects in two orientations.

B. Positron states

We calculated the positron states in 9 cation vacancy systems that can be divided into three groups: regular mono-vacancies $V_{\text{Ga}1}$ and $V_{\text{Ga}2}$, split Ga vacancies $V_{\text{Ga}}^{\text{ia}}$, $V_{\text{Ga}}^{\text{ib}}$ and $V_{\text{Ga}}^{\text{ic}}$, and hydrogenated split Ga vacancies $V_{\text{Ga}}^{\text{ib}-1\text{H}}$, $V_{\text{Ga}}^{\text{ib}-2\text{H}}$, $V_{\text{Ga}}^{\text{ic}-1\text{H}}$ and $V_{\text{Ga}}^{\text{ic}-2\text{H}}$. We chose systems that are simple and predicted to be energetically favorable ($V_{\text{Ga}}^{\text{ia}}$, $V_{\text{Ga}}^{\text{ib}}$, $V_{\text{Ga}}^{\text{ic}}$) [7], or suggested via experiments ($V_{\text{Ga}}^{\text{ib}}$, $V_{\text{Ga}}^{\text{ic}}$, $V_{\text{Ga}}^{\text{ib}-2\text{H}}$) [9, 10]. At Fermi level close to the conduction band, the charge state of "clean" cation monovacancies is predicted as -3 , after passivation with one hydrogen ($V_{\text{Ga}}^{\text{ib}-1\text{H}}$ and $V_{\text{Ga}}^{\text{ic}-1\text{H}}$) the charge state is predicted as -2 , and with 2 hydrogen atoms ($V_{\text{Ga}}^{\text{ib}-2\text{H}}$ and $V_{\text{Ga}}^{\text{ic}-2\text{H}}$) the charge state is predicted as -1 [6, 7].

The calculated shapes of the density of the localized positron state can be also divided into three groups. The regular vacancies ($V_{\text{Ga}1}$ and $V_{\text{Ga}2}$) exhibit a sphere-like positron density as is typical of large enough vacancy defects, as illustrated in Fig. 9. In the case of vacancies with two symmetric open volumes, $V_{\text{Ga}}^{\text{ib}}$, $V_{\text{Ga}}^{\text{ic}}$, $V_{\text{Ga}}^{\text{ib}-2\text{H}}$ and $V_{\text{Ga}}^{\text{ic}-2\text{H}}$, the positron localizes in the calculation equally into both half-vacancies. The positron density bodies of two symmetric half-vacancies are connected with a bridge of positron density with 5 % of the maxi-

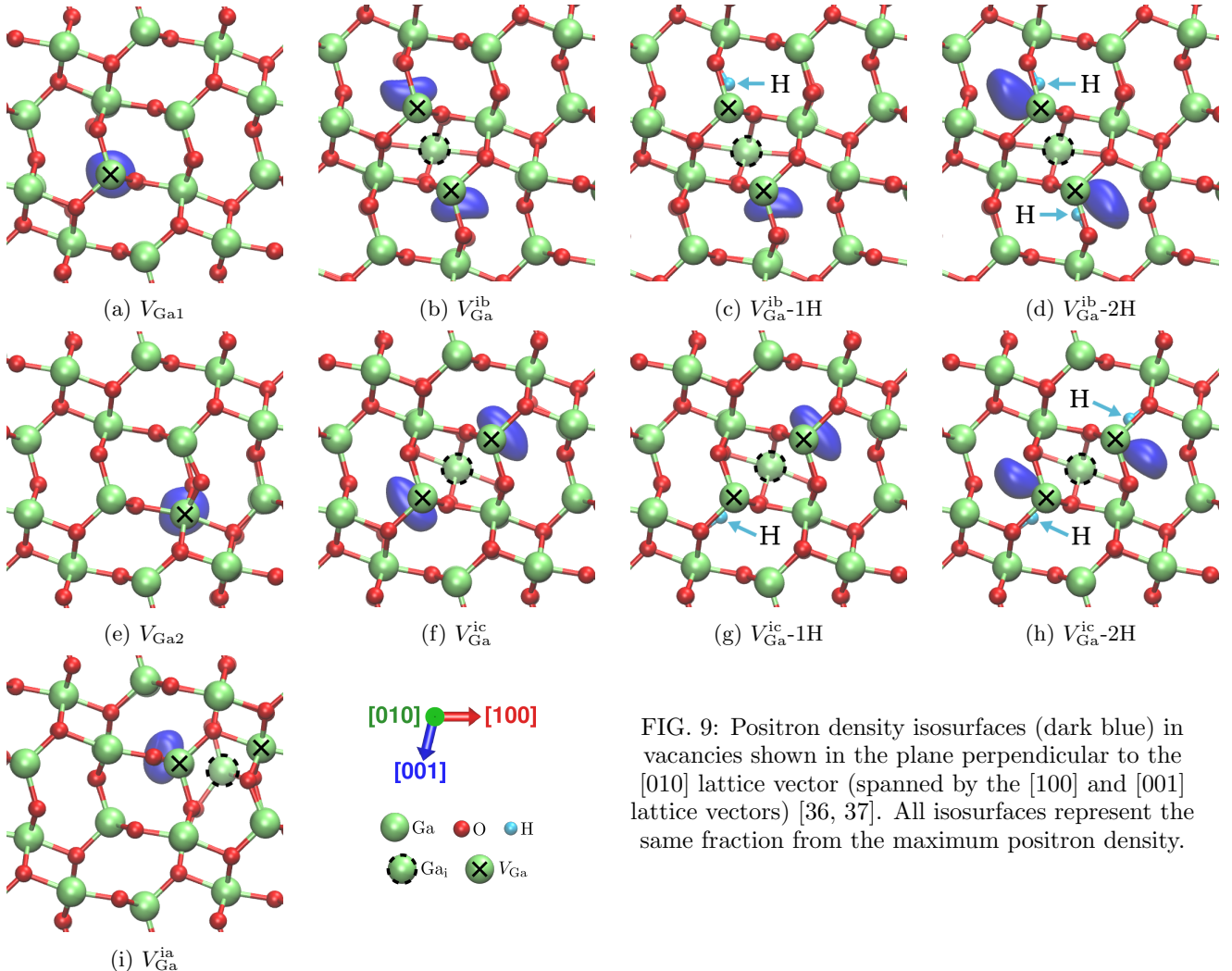


FIG. 9: Positron density isosurfaces (dark blue) in vacancies shown in the plane perpendicular to the [010] lattice vector (spanned by the [100] and [001] lattice vectors) [36, 37]. All isosurfaces represent the same fraction from the maximum positron density.

imum density value. Hence the half-vacancies can be considered as being part of the same potential well (and not two separate indistinguishable potential wells). In split Ga vacancies where the symmetry is broken, $V_{\text{Ga}}^{\text{ia}}$ (different Ga sites), $V_{\text{Ga}}^{\text{ib}}-1\text{H}$ or $V_{\text{Ga}}^{\text{ic}}-1\text{H}$, the positron localizes into the larger open volume. In the case of $V_{\text{Ga}}^{\text{ib}}-1\text{H}$ and $V_{\text{Ga}}^{\text{ic}}-1\text{H}$, the hydrogen occupies one of the half-vacancies and the positron localizes into the other half-vacancy. The positron density has a similar shape in these single-hydrogen half-vacancies as in the respective split Ga vacancies without hydrogen. In the split Ga vacancies with 2 hydrogen atoms, $V_{\text{Ga}}^{\text{ib}}-2\text{H}$ and $V_{\text{Ga}}^{\text{ic}}-2\text{H}$, the hydrogen atoms occupy both "half-vacancies" making the situation symmetric again. As the positive charge of the hydrogen core occupies the center of the open volume it pushes the positron away from the center, changing the location and shape of the positron density compared to the split Ga vacancies without hydrogen.

C. Positron lifetimes

The calculated measurable quantities, the positron lifetimes (Table II) and Doppler broadening signals, follow roughly the same division of shape of the positron densities described in the previous section. The "regular" vacancies ($V_{\text{Ga}1}$ and $V_{\text{Ga}2}$) have the largest open volume and exhibit longest positron lifetimes, 54 ps above the calculated positron lifetime of 135 ps in the $\beta\text{-Ga}_2\text{O}_3$ lattice. Due to historical naming conventions we denote the positron lifetime in the lattice as τ_B where the subscript B refers to "bulk". It should be noted that the predictive power of the state-of-the-art theoretical calculations in terms of the absolute scale of positron lifetimes (and (S, W) parameters) is low due to the different choices of approximations resulting in a wide range of, e.g., lattice lifetimes. Instead, differences between localized states and the lattice state can be compared in great detail between experiment and theory [11].

In split Ga vacancies $V_{\text{Ga}}^{\text{ia}}$, $V_{\text{Ga}}^{\text{ib}}$ and $V_{\text{Ga}}^{\text{ic}}$, the remaining open volume is smaller and the positron lifetime is 25 – 36 ps longer than in the lattice. The addition of a

single hydrogen atom to $V_{\text{Ga}}^{\text{ib}}$ or $V_{\text{Ga}}^{\text{ic}}$ makes the positron to localize in the empty half of the split-vacancy without major changes to the positron density distribution, and the positron lifetime for $V_{\text{Ga}}^{\text{ib}}\text{-1H}$ and $V_{\text{Ga}}^{\text{ic}}\text{-1H}$ is essentially the same as for the same defects without hydrogen. Adding a second hydrogen atom significantly reduces the open volume and the resulting positron lifetimes for $V_{\text{Ga}}^{\text{ib}}\text{-2H}$ and $V_{\text{Ga}}^{\text{ic}}\text{-2H}$ are only 11 – 15 ps longer than τ_B .

TABLE II: Calculated positron lifetimes and Doppler broadening signal anisotropies. The anisotropy spans are calculated dividing the maximum and minimum (S, W) parameters by the respective parameter of the $\beta\text{-Ga}_2\text{O}_3$ lattice in the [001] direction.

| System | Positron lifetime (ps) | Anisotropy in | |
|---------------------------------------|-------------------------|---------------|-------------|
| | | S | W |
| Lattice | 135 | 1.000 - 1.020 | 0.97 - 1.00 |
| $V_{\text{Ga}1}$ | $\tau_B + 54$ | 1.018 - 1.040 | 0.90 - 0.97 |
| $V_{\text{Ga}2}$ | $\tau_B + 54$ | 1.022 - 1.038 | 0.91 - 0.96 |
| $V_{\text{Ga}}^{\text{ia}}$ | $\tau_B + 25$ | 1.005 - 1.023 | 0.95 - 0.99 |
| $V_{\text{Ga}}^{\text{ib}}$ | $\tau_B + 32$ | 0.998 - 1.032 | 0.93 - 1.02 |
| $V_{\text{Ga}}^{\text{ib}}\text{-1H}$ | $\tau_B + 27$ | 0.991 - 1.031 | 0.92 - 1.05 |
| $V_{\text{Ga}}^{\text{ib}}\text{-2H}$ | $\tau_B + 11$ | 1.002 - 1.023 | 0.93 - 0.99 |
| $V_{\text{Ga}}^{\text{ic}}$ | $\tau_B + 36$ | 0.998 - 1.031 | 0.92 - 1.03 |
| $V_{\text{Ga}}^{\text{ic}}\text{-1H}$ | $\tau_B + 32$ | 0.986 - 1.031 | 0.92 - 1.08 |
| $V_{\text{Ga}}^{\text{ic}}\text{-2H}$ | $\tau_B + 15$ | 0.999 - 1.026 | 0.92 - 1.00 |
| $V_{\text{O}1}$ | does not trap positrons | | |
| $V_{\text{O}2}$ | does not trap positrons | | |
| $V_{\text{O}3}$ | does not trap positrons | | |

D. Anisotropy of Doppler broadening signals

Figure 10 shows the calculated (S, W) parameters of the considered defects, normalized by the (S, W) parameters of $\beta\text{-Ga}_2\text{O}_3$ in the [001] lattice direction (the direction of the smallest S parameter in the $\beta\text{-Ga}_2\text{O}_3$ lattice). The figure uses the notation introduced in Fig. 5 for square, triangle and circle to represent [100], [010] and [001] lattice directions, respectively, and full, dashed and dotted curves to represent (S, W) parameters on the geodesics between the [100] and [010], [010] and [001], and [001] and [100] directions, respectively. The grey shadow illustrates the (S, W) of the $\beta\text{-Ga}_2\text{O}_3$ lattice (from Fig. 5). The $\beta\text{-Ga}_2\text{O}_3$ lattice and all the considered defects have their maximum S parameters in the [010] direction, while the smallest S parameter lies in [100]-[001] plane, in most cases in the vicinity of the [001] lattice direction. The defect ratio curves for the different directions are shown in the Appendix. They exhibit the same general behavior as the (S, W) parameters and are not discussed here in more detail as their correct use in defect identification requires a well-defined experimental reference sample. Figure 10 visualizes the anisotropy issue already evident from the (S, W) parameter values

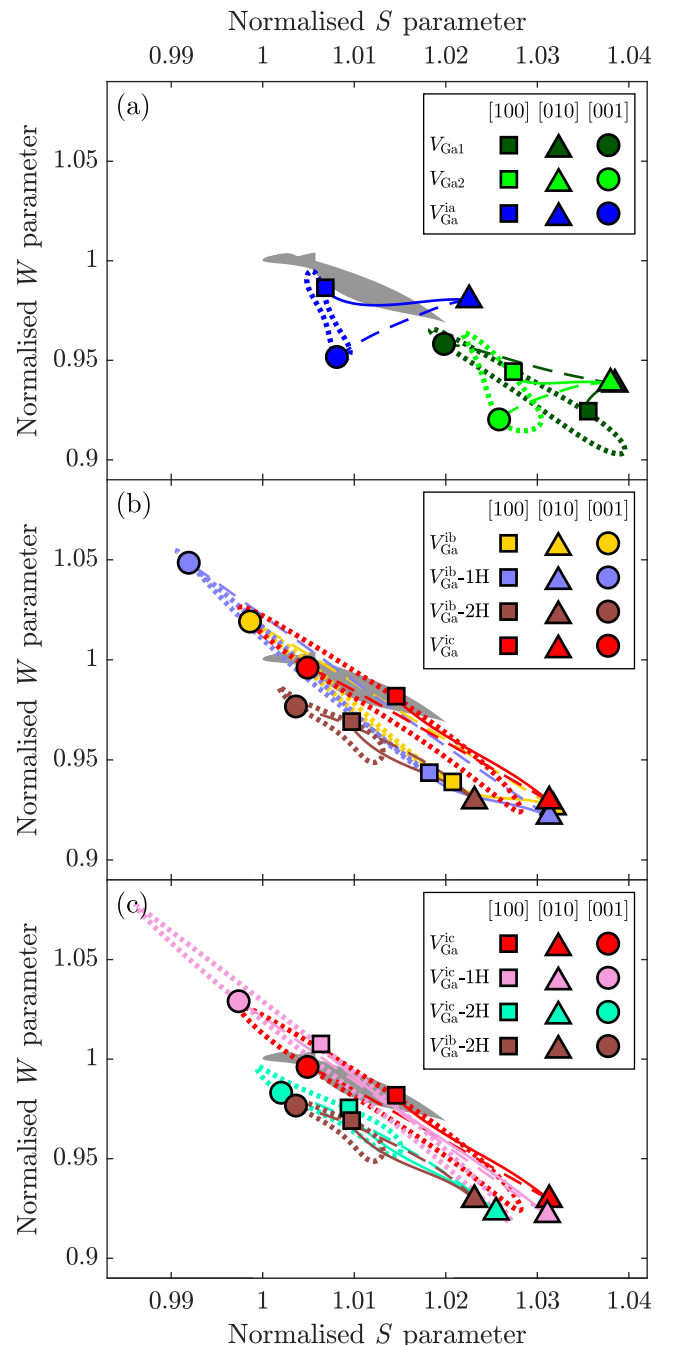


FIG. 10: The calculated (S, W) parameters in vacancies normalized to (S, W) parameters of $\beta\text{-Ga}_2\text{O}_3$ lattice in the [001] lattice direction. The grey shadow illustrates the (S, W) parameters of the $\beta\text{-Ga}_2\text{O}_3$ lattice from Fig. 5. The same notation is used for full, dashed and dotted curves to show (S, W) parameters on the geodesics between [100] and [010], [010] and [001], and [001] and [100], respectively.

shown in Table II. All of the considered vacancy defects exhibit at least as large an anisotropy in the Doppler signals as the β -Ga₂O₃ lattice, in contrast to what has been experimentally observed and/or theoretically calculated for materials such as Si, GaN, and ZnO where vacancies exhibit similar or smaller magnitude of anisotropy as the lattice [43, 45]. In addition, the (S, W) parameters of many of the defects completely overlap with those of the β -Ga₂O₃ lattice.

The most distinct shape of anisotropies is exhibited by $V_{\text{Ga}1}$, $V_{\text{Ga}2}$ and $V_{\text{Ga}}^{\text{ia}}$ as their collection of (S, W) parameters reminds a right-pointing triangle (Fig. 10). The $V_{\text{Ga}1}$ and $V_{\text{Ga}2}$ have the highest S parameters of the monovacancy-sized defects and their S parameters span roughly from 1.02 to 1.04, see Table II. The two regular mono-vacancies share the same (S, W) parameters in the [010] lattice direction, while in the [100] and [001] directions the anisotropy of their Doppler parameters has a different shape and the minimum and maximum S parameters in the [100]-[001] plane are in different lattice directions. The shape of the anisotropy of $V_{\text{Ga}}^{\text{ia}}$ reminds $V_{\text{Ga}2}$ but $V_{\text{Ga}}^{\text{ia}}$ has smaller S and higher W parameters and it almost fully overlaps with the β -Ga₂O₃ lattice, with the S parameter spanning from 1.005 to 1.023.

A second recognizable group is defects with anisotropy along the diagonal, namely the split Ga vacancies $V_{\text{Ga}}^{\text{ib}}$ and $V_{\text{Ga}}^{\text{ic}}$ together with their singly hydrogenated versions $V_{\text{Ga}}^{\text{ib}}\text{-1H}$ and $V_{\text{Ga}}^{\text{ic}}\text{-1H}$ (see Figs. 10b and 10c). The calculated Doppler broadening results predict that in the [100]-[001] plane their (S, W) parameters swing all the way from the smallest S parameter up to almost the maximum S parameter in the [010] lattice direction. The $V_{\text{Ga}}^{\text{ib}}$, $V_{\text{Ga}}^{\text{ic}}$, $V_{\text{Ga}}^{\text{ib}}\text{-1H}$ and $V_{\text{Ga}}^{\text{ic}}\text{-1H}$ have the same (S, W) parameters in the [010] lattice direction. The (S, W) parameters of the split Ga vacancies $V_{\text{Ga}}^{\text{ib}}$ and $V_{\text{Ga}}^{\text{ic}}$ (Fig 10b) span from 0.998 to 1.032 in S and from 0.92 to 1.03 in W , covering the (S, W) range of the β -Ga₂O₃ lattice completely. They also overlap with each other very strongly. However, in the [100]-[001] plane $V_{\text{Ga}}^{\text{ib}}$ has the smallest S parameter close to the [001] direction and maximum in [100] whereas $V_{\text{Ga}}^{\text{ic}}$ reaches similar (S, W) parameter values but in directions which are rotated 45° from the [100] lattice vector towards the [001] lattice vector. The (S, W) parameters in $V_{\text{Ga}}^{\text{ic}}$ in the [100] and [001] lattice directions are roughly in the middle of the total (S, W) parameter range of the [100]-[001] plane.

Adding one hydrogen to the split Ga vacancies $V_{\text{Ga}}^{\text{ib}}$ and $V_{\text{Ga}}^{\text{ic}}$ localizes the positron to only one of the half-vacancies without dramatically changing the shape of the positron density and with only a minor effect on the positron lifetime. In Doppler broadening results, the addition of one hydrogen increases the anisotropy span but keeps the (S, W) parameters of the [010] lattice direction intact. The (S, W) parameters of the [100] and [001] lattice directions, and the whole [100]-[001] plane, are spread towards smaller S and larger W parameters. $V_{\text{Ga}}^{\text{ic}}\text{-1H}$ is found to have the smallest S parameter (0.986), significantly smaller than that in the β -Ga₂O₃ lattice, and

the S parameters of $V_{\text{Ga}}^{\text{ib}}\text{-1H}$ and $V_{\text{Ga}}^{\text{ic}}\text{-1H}$ span from 0.991 to 1.031. Adding a second hydrogen atom changes the shape of anisotropy of $V_{\text{Ga}}^{\text{ib}}\text{-2H}$ and $V_{\text{Ga}}^{\text{ic}}\text{-2H}$ and they become almost indistinguishable. Their shape of anisotropy is somewhat similar to the β -Ga₂O₃ lattice but they do not overlap with the lattice (S, W) parameters. The whole range of the anisotropy is still much larger than in the lattice, and the S parameter spans roughly from 1.00 to 1.025.

V. COMPARISON TO EXPERIMENTS

We compare the results of our theoretical calculations to experimental results obtained in two semi-insulating single crystal β -Ga₂O₃ bulk samples (S1 and S2 in the following) that are grown by the Czochralski method and doped with Mg [25, 46]. The surface of the plate-like sample S1 is in the (100) crystal plane and the surface of S2 in the (010) plane. To exclude possible experimental artefacts, the Doppler broadening of the positron-electron annihilation radiation was measured in the samples in two different ways, with a slow positron beam and with a fast positron setup.

The fast positron measurements were performed on two identical pieces of S1 in the three lattice directions of the standard conventional unit cell of β -Ga₂O₃, and along the geodesics connecting the lattice directions with a 10° step. In the fast positron setup, a high-purity Ge (HPGe) detector with energy resolution of 1.15 keV at 511 keV was used to record the annihilation photons emitted from two sample pieces with a positron source sandwiched in between. The positron source with 1 MBq of activity was composed of ²²Na encapsulated in 1.5 μm thick Al-foil. The amount of source annihilations was determined with positron lifetime measurements (not discussed in detail in this work) to be less than 4%. The distance between the sample-source sandwich and the detector was 35 cm yielding an angular resolution of about 10° as defined by the solid angle covered by the detector crystal. The crystal orientations of the samples were determined by X-ray diffraction measurements. The sample-source sandwich was rotated to collect annihilation spectra in all desired directions. The (S, W) parameter windows were set as 0 – 0.45 a.u. for the S and to 1.54 – 4.07 a.u. for the W parameter. A total of 10⁶ counts was recorded for each spectrum.

In the slow positron beam experiments, two unspecified perpendicular directions within the surface plane of the sample were measured in samples S1 and S2 [25] with two HPGe detectors that have an energy resolution of 1.25 keV at 511 keV. In S1, the measurement directions were in the plane spanned by the [010] and [001] lattice vectors, while for S2, the measurements were performed in the plane spanned by the [100] and [001] lattice vectors. The aspect ratio is clearly different from the fast positron setup as the detectors are only at a distance of roughly 3 cm from the sample. The (S, W) parameter values were

acquired at positron implantation energy of 25 keV, corresponding to mean stopping depth 1.2 μm , so that the back-diffusion generated annihilations at the surface do not affect the data. The same (S, W) parameter windows were applied as in the fast positron experiments.

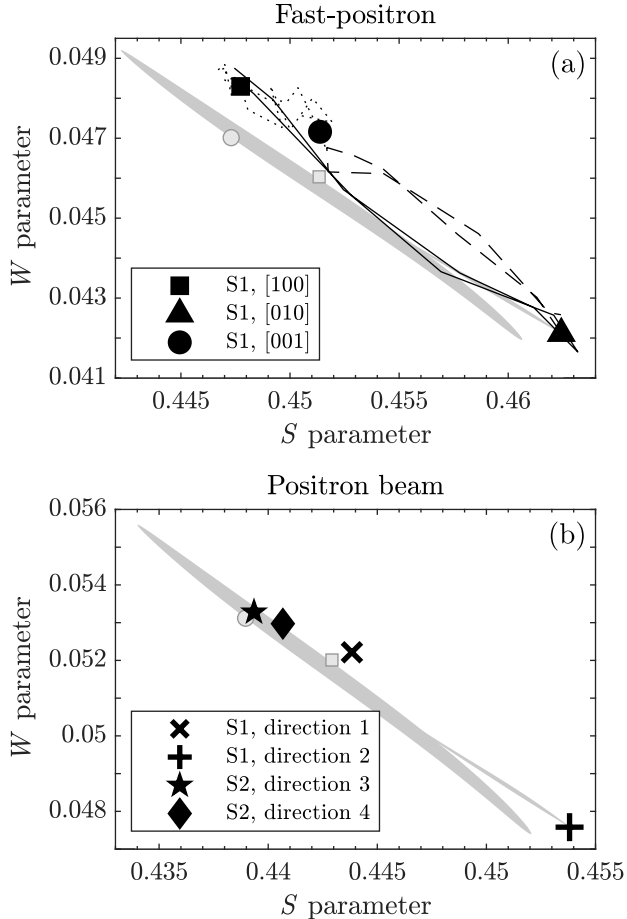


FIG. 11: Experimental (S, W) parameters of the studied $\beta\text{-Ga}_2\text{O}_3$ samples. The grey shadow illustrates the calculated (S, W) parameters of $V_{\text{Ga}}^{\text{ic}}\text{-1H}$, the defect with the largest anisotropy, as shown in Fig. 10. (a) Standard fast positron measurement of sample S1 in the lattice vector directions and on the geodesics between them with the notation introduced in Fig. 5. (b) Sample S1 (100) and S2 (010) measured with a slow positron beam at an acceleration voltage of 25 kV. Two directions perpendicular to the sample surface normal were measured for both samples.

The results of the fast positron measurements are shown in Fig. 11a. The experimental (S, W) parameter values in the lattice directions [100], [010] and [001], and along the geodesics between them, behave almost linearly. The (S, W) parameters of the [100] and [001] directions are rather close to each other while the [010] direction has clearly the highest S parameter. The positron beam measurement shows features similar to the fast

positron measurement (Fig. 11b). It is natural that the absolute (S, W) parameter values differ from the fast positron measurement: these two experiments were done in different setups with different detectors and measurement geometries. In addition, in the fast positron measurement there is a $\lesssim 4\%$ isotropic source contribution to the annihilations. The measurement directions 1 and 2 of sample S1 share a close resemblance to the [100] and [010] lattice directions of the fast positron experiment, respectively. The ratio of the (S, W) parameters of directions 1 and 2 are 1.023 for the S and 0.90 for the W parameter, while the corresponding ratios of [100] and [010] crystal directions in the fast positron measurement are 1.025 and 0.90, respectively. This suggests that the directions 1 and 2 of sample S1 are close to [100] and [010] lattice directions. In sample S2, directions 3 and 4 differ less than [100] and [001] suggesting that the measurement directions are slightly off from [100] and [001] lattice directions.

The overall magnitude of the anisotropy observed in the positron beam measurement (S1 direction 2, S2 direction 3) is 1.033 for the S and 0.89 for the W parameter. This is similar in the fast positron measurement of sample S1, where the overall magnitude is 1.035 for the S and 0.84 for the W parameter. Here the anisotropy is defined as the largest (smallest) S (W) parameter divided by the smallest (largest) S (W) parameter. Figure 11 also shows the theoretically calculated (S, W) parameter of $V_{\text{Ga}}^{\text{ic}}\text{-1H}$, the defect with the largest overall anisotropy, with a grey shadow and grey markers along the lattice vectors. As discussed in previous sections, the lack of reference $\beta\text{-Ga}_2\text{O}_3$ material prevents normalizing the experimental (S, W) parameters, and the comparison of normalized theoretical and experimental (S, W) parameters. Instead, we shifted the (S, W) parameters of the theoretical calculations so that the [010] lattice direction matches the maximum S (and minimum W) parameter of the experiments. The operation does not affect the shape or relative magnitude of the anisotropy and allows us to compare the experimental and theoretical anisotropies. Clearly the scale of the anisotropy in the Doppler signals is the same in experiments and theory, and an order of magnitude higher than observed in other semiconductors [42, 43], comparable to the anisotropy in graphite [38]. Interestingly, the experimental anisotropy is comparable in magnitude to that in $V_{\text{Ga}}^{\text{ic}}\text{-1H}$, which is three times larger than that of the $\beta\text{-Ga}_2\text{O}_3$ lattice. Note that the defect predicted to have the lowest formation energy [6], namely the $V_{\text{Ga}}^{\text{ib}}\text{-2H}$, has an overall anisotropy that is twice that of the $\beta\text{-Ga}_2\text{O}_3$ lattice, but somewhat smaller than the experimental anisotropy. These observations suggest that the single crystal $\beta\text{-Ga}_2\text{O}_3$ samples contain high concentrations of (hydrogenated) split Ga vacancies.

Figure 11 shows that from the point of view of the anisotropy of the Doppler signals, experiment and theory are in excellent agreement in three aspects: (i) the maximum S (minimum W) are found in the [010] direction,

(ii) the general shape of the anisotropy follows the same trend and (iii) the overall magnitude of the anisotropy is colossal compared to other studied 3D semiconductor crystals. There is, however, a small but systematic difference that needs to be addressed. The calculations predict the S parameter in the [001] lattice direction to be smaller than in the [100] direction for nearly all of the considered defects, while the positron experiments (including also our unpublished results) consistently show the [100] lattice direction to have lower S parameter than the [001] direction. In both experiment and theory, the [100] and [001] directions are similar in the sense that they produce (S, W) parameters that are quite close to each other and clearly far away from the [010] direction. We found that if the positron signals are calculated using different published $\beta\text{-Ga}_2\text{O}_3$ unit cells, the (S, W) parameters of the [100] and [001] lattice directions change to a certain degree. This is illustrated in Fig. 12 where we show the calculated Doppler signals in the $\beta\text{-Ga}_2\text{O}_3$ lattice using the computationally determined unit cell [6] used throughout this work and in an experimental unit cell determined in Ref. 47. The exact locations of atoms in these two unit cells are slightly different and, unlike in materials with cubic or hexagonal crystal structures, ideal atomic structures based on symmetry cannot be used.

We assign the slight discrepancy between theory and experiments in the relative (S, W) parameters in the [100] and [001] lattice directions to the apparent sensitivity of the Doppler signal in these lattice directions to the exact structure of the unit cell used in calculation. Clearly detailed X-ray experiments are needed on state-of-the-art $\beta\text{-Ga}_2\text{O}_3$ materials to resolve the exact crystal structure, which may not be the same for, *e.g.*, strained thin films and single crystals. Also, when comparing directly experimental and theoretical (S, W) results resulting from rotating the sample, we have to stress that even though we take into account the experimental energy resolution of the detectors, our simulations do not yet account for the finite size of the detectors and integration over a finite solid angle especially in measurements made with slow positron beams. Including the effect of a proper angular resolution function in modeling can be expected to smoothen the behavior of the (S, W) values in graphs such as Fig. 10 and limit the extrema especially if they occur only in specific directions covered by a small solid angle (see, for example, Fig. 5a).

VI. DISCUSSION

The colossal anisotropy of positron-electron momentum distributions in $\beta\text{-Ga}_2\text{O}_3$ that leads to strongly direction-dependent data in Doppler broadening experiments is prone to produce incomprehensible results if its existence is neglected. Even when taken into account, the strong overlap of vacancy and lattice (S, W) parameters makes interpreting the results challenging. If the

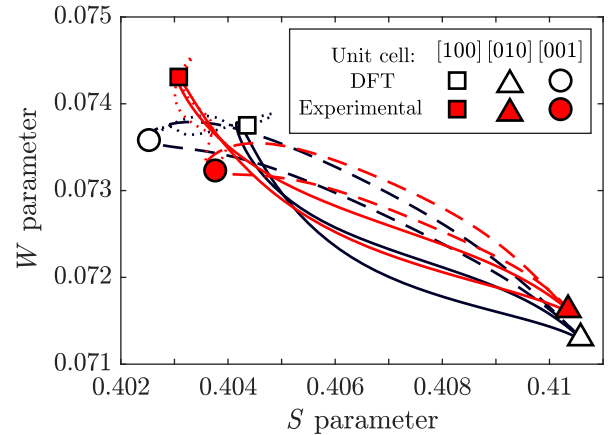


FIG. 12: The Doppler signals calculated in the $\beta\text{-Ga}_2\text{O}_3$ lattice using two different unit cells, a computational [6] and experimental unit cell [47]. The slightly different atomic locations lead to differences in calculations in the [001] and [100] directions.

exact sample orientation (with respect to the crystal lattice) is not known in experiments, there is a severe risk of erroneous conclusions. For example, the (S, W) parameter values near the $\beta\text{-Ga}_2\text{O}_3$ lattice signal in the [010] direction can also originate from many of the defects considered in this work, if measured in a suitable lattice direction. In addition, as seen in Fig. 10, most of the defect-related and anisotropy-related phenomena are aligned on the same diagonal in the (S, W) plane, making their distinction impossible if the experiments are not carefully designed. Comparing Doppler broadening results in $\beta\text{-Ga}_2\text{O}_3$ samples makes sense only when care is taken to measure all samples in the exact same lattice direction, a precaution that is not necessary in other semiconductors.

In spite of all the difficulties, the colossal anisotropy brings also benefits. The differently behaving anisotropy for the different types of vacancy defects may be used for defect identification, in particular when a suitable reference (a sample that could be interpreted to produce positron annihilation signals representing the $\beta\text{-Ga}_2\text{O}_3$ lattice) does not exist and detailed identification via relative (S, W) parameters or ratio curves is not possible. In the following, we discuss how to take advantage of the colossal anisotropy and also try to shed light on its origins.

A. Defect identification

The strong vacancy-lattice overlap and colossal anisotropy of the Doppler broadening signals make defect identification difficult even if the experimental (S, W) parameters of the lattice were available. It is important to

keep in mind that positron annihilation spectroscopy is a comparative methodology in the sense that detailed defect identification and quantification relies on the availability of reference material where positrons annihilate predominantly in the delocalized state in the lattice, that is where no positron trapping at vacancy defects is observed. Identification of such a piece of reference material requires (i) that the positron lifetime spectrum has only one component, (ii) that this lifetime is reasonable (short enough) compared to the atomic and mass densities of the material, (iii) that the temperature dependence of the positron lifetime is negligible, and potentially only shows effects from thermal expansion of the lattice, (iv) that the positron diffusion length (when it can be determined) is long enough, close to 200 nm, and (v) that the other physical characteristics of the sample are such that it is reasonable to interpret the situation as one where the overall concentration of neutral and negative vacancy-type defects is clearly less than $\sim 10^{16} \text{ cm}^{-3}$. So far, systematic studies of the positron lifetime in $\beta\text{-Ga}_2\text{O}_3$ have not been performed, and only conditions (i) and (ii) are fulfilled: $\beta\text{-Ga}_2\text{O}_3$ single crystals have been reported to show a single positron lifetime component measured at room temperature of about 175 – 180 ps [23, 24]. We proceed without assuming the knowledge of the experimental (S, W) parameters of the $\beta\text{-Ga}_2\text{O}_3$ lattice.

We start comparing the experimental (S, W) parameters (Fig. 11) to the calculated (S, W) parameters (Fig. 10) by observing that the magnitude of the experimental anisotropy is 1.035 for S and 0.84 for the W parameter, almost double the S anisotropy and 5-fold the W anisotropy calculated for the $\beta\text{-Ga}_2\text{O}_3$ lattice. This strongly suggests that the experimental positron data obtained in the $\beta\text{-Ga}_2\text{O}_3$ single crystal (that only shows a single lifetime component of ~ 185 ps) is dominated by defect signals, which means that the concentration of positron-trapping vacancy defects in the sample is at least $\sim 10^{18} \text{ cm}^{-3}$. We discard the possibility of a major contribution from $V_{\text{Ga}1}$, $V_{\text{Ga}2}$ and $V_{\text{Ga}}^{\text{ia}}$ in the experimental data as the shape of the anisotropy is clearly different. Fig. 11 shows the calculated (S, W) parameters of the defect with the largest anisotropy, $V_{\text{Ga}}^{\text{ic}}\text{-1H}$, as a grey shadow. The shape of the experimental anisotropy is close to the shape of all the other calculated defects, that is split Ga vacancies of *ib* and *ic* type, with and without hydrogen. In the experimental results, the (S, W) parameters in the [100] and [001] lattice directions are much closer to each other than the parameters in the [010] direction, which suggests that the experimental data resemble more the $V_{\text{Ga}}^{\text{ic}}$ -type split Ga vacancies. However, as the calculated (S, W) parameters vary a lot along the geodesics connecting [100] and [001] in the $V_{\text{Ga}}^{\text{ib}}$ -type split Ga vacancies, this is not as strong an argument as the one ruling out the first set of defects. The magnitude of the calculated anisotropy for the doubly hydrogenated split Ga vacancies is smaller than that in the experiments, suggesting that the dominant contribution to the experimental data could indeed come from the clean and singly

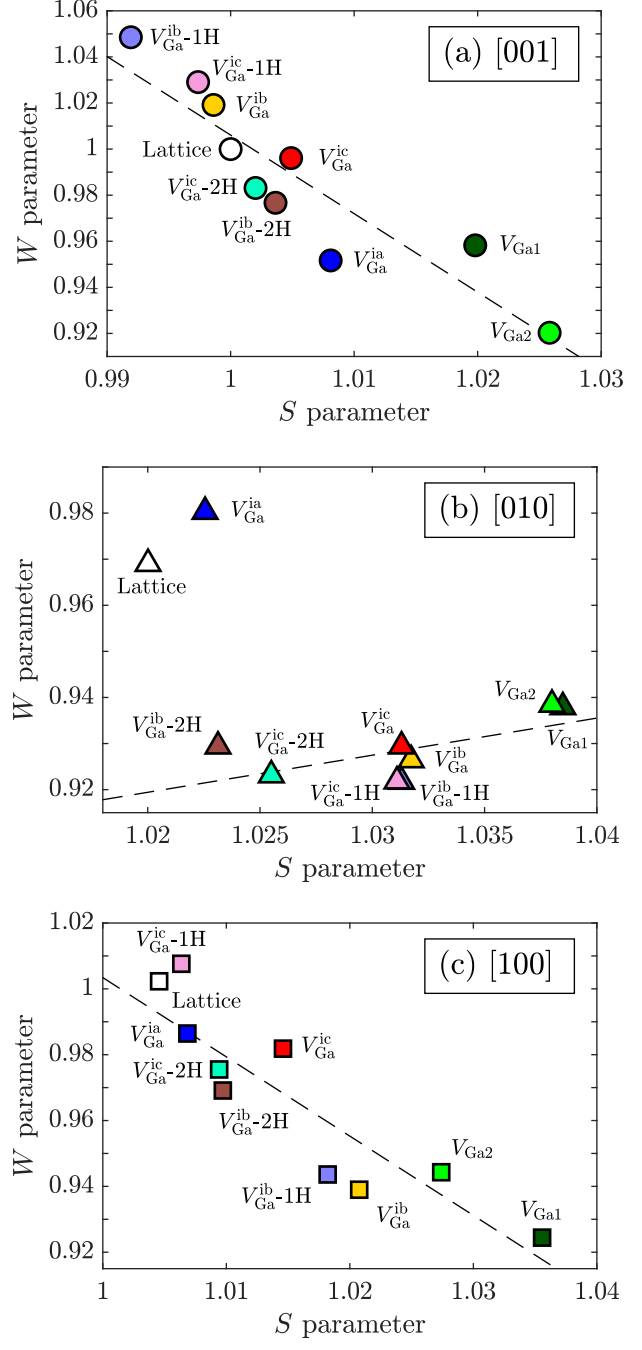


FIG. 13: Calculated (S, W) parameters in the $\beta\text{-Ga}_2\text{O}_3$ lattice and the vacancy defects sorted in (a) [001], (b) [010] and (c) [100] lattice directions to illustrate the different behaviour in slow positron beam experiments in selected directions. The (S, W) parameters are normalized to the (S, W) parameters of $\beta\text{-Ga}_2\text{O}_3$ lattice in the [001] lattice direction. The lines are drawn to guide the eye.

hydrogenated split Ga vacancies. The assignment of experimentally observed anisotropy of the Doppler signals to $V_{\text{Ga}}^{\text{ic}}$ -related defects is also supported by the recent theoretical and experimental work: $V_{\text{Ga}}^{\text{ic}}$ has been predicted to have the lowest formation energy among clean mono-vacancy type defects [7], and the existence of $V_{\text{Ga}}^{\text{ic}}$ was observed with STEM [10]. The fact that these defects could be found by STEM agrees well with the estimate from positron annihilation: in both experiments, the split Ga vacancy concentration needs to be at least 10^{18} cm^{-3} .

Performing positron experiments in multiple orientations to detect the anisotropy is not always feasible due to time constraints, or even possible. For example, in slow positron beam studies the measurement geometry is fixed, typically allowing for experiments either in the plane of the sample surface or perpendicular to it, but not both. Measuring multiple orientations with a slow positron beam for several samples is excessively time consuming. In addition, the angular resolution in such experiments is poor due to the short sample-detector distance. Hence, measuring two perpendicular directions is a reasonable approach for utilizing the positron signal anisotropy in slow positron beam studies. The surface orientation of the samples is relevant for positron studies, and it is important to know the in-plane orientation as well in order to choose the appropriate measurement geometry. Figure 13 illustrates how the normalized (S, W) of $\beta\text{-Ga}_2\text{O}_3$ lattice and defects behave in the [001], [010] and [100] lattice directions. The calculated (S, W) parameters in those lattice directions have different overall trends and magnitudes of differences between defects vary. The regular mono-vacancies $V_{\text{Ga}1}$ and $V_{\text{Ga}2}$ show the largest S parameter in all lattice directions the relative positions of the (S, W) parameters of the other defects change from one direction to another.

The trends of the (S, W) parameters in the [001] and [100] lattice directions are rather similar and follow a diagonal line. As discussed in the previous section, the details of the relative (S, W) parameter positions in these two directions may depend on the exact atomic positions in the unit cell. There is, however, an important aspect that can be seen in the [001] data in Fig. 13a and is even more pronounced in Fig. 10: some of the defects, such as $V_{\text{Ga}}^{\text{ib}}\text{-H}$ and $V_{\text{Ga}}^{\text{ic}}\text{-H}$, are characterised by a shift of the (S, W) parameters towards the upper left corner from the $\beta\text{-Ga}_2\text{O}_3$ lattice point, even when measured in the same direction. This needs to be taken into account when attempting an interpretation of experimental positron data in $\beta\text{-Ga}_2\text{O}_3$, as usually the lattice produces the lowest S and highest W parameters. The reason for this unusual behavior is discussed in the Appendix. In the [010] direction, the (S, W) parameters of the defects behave completely differently and set on an nearly horizontal line (excluding $V_{\text{Ga}}^{\text{ia}}$) where the S parameter roughly follows the lifetime and the size of the open volume. Importantly, the (S, W) parameters of the defects are no longer aligned with those of the lattice, providing additional means for distinguishing defect-related phenomena

from anisotropy-related phenomena in the experimental data.

It is worth considering the interpretations and discussion of the experimental results presented in Refs. 24 and 25 in the light of our theoretical calculations. Most of the experimental data in those reports were measured with a slow positron beam in thin films grown on (100) oriented $\beta\text{-Ga}_2\text{O}_3$ substrates. After the publication of those reports, it was found that the measurements were performed in a "low- S " direction that probably is close to the [001] lattice direction (as the other direction in that plane is [010], a "high- S " direction). The (S, W) data in Refs. 24 and 25 fall on the dashed line (or its extension) presented in Fig. 13a, if the "bulk" measurement data point is associated to any of the ib or ic type split Ga vacancies or the lattice. The data points in the Si-doped thin film samples studied in Ref. 24 are somewhat further away from the bulk point than the $V_{\text{Ga}1}$ $V_{\text{Ga}2}$, while the Sn-doped and undoped thin film samples (Ref. 25) are all very close to the bulk point. In those reports this behavior of the data is associated to different levels of hydrogenation of the samples due to different precursors in the synthesis. Our results on the split Ga vacancies bring more detail to this interpretation. We suggest that in the Sn-doped and undoped $\beta\text{-Ga}_2\text{O}_3$ thin films the positron data are dominated by (hydrogenated) split Ga vacancies, in line with the directional dependence of the signals seen in Ref. 25 and the Sn-type split Ga vacancies observed in Ref. 10, where Sn substitutes for the Ga atom relaxing to the interstitial position. This relaxation does not happen when Si substitutes for Ga [6, 7], and allows for the formation of regular Ga mono-vacancies observed in the experiments. This interpretation answers the question raised in those reports concerning the low formation energy of Ga vacancies - indeed experiments indicate that Ga vacancies are abundant in all $\beta\text{-Ga}_2\text{O}_3$ samples. Further, recent calculations [48] predict that the split Ga vacancies can accommodate three H atoms and become neutral and non-compensating. This provides a plausible solution to the electrical compensation question: split Ga vacancies are present at high concentrations in n -type material, but they only act as efficient compensating centers when not strongly hydrogenated.

B. Anisotropies of the positron density and annihilation radiation

The momentum density of annihilating pairs measured in a Doppler broadening experiment reflects the anisotropy present in the ionic and electronic structures of the lattice. It can be viewed as the electron momentum density "as seen by the positron". The possible anisotropy of the annihilation signal of the delocalized lattice state is affected by a number of factors, including:

1. The electron momentum density of the host lattice (in the absence of any positrons, as in X-ray Compton scattering experiments [33]). The anisotropy of

the lattice itself can result in an anisotropic electron momentum density.

2. The momentum density of the positron. Confinement in one or more directions can lead to a corresponding broadening.
3. The positron density distribution in the lattice and its overlap with the electronic orbitals. In the delocalized state in a defect-free lattice, the positron probes the interstitial region far away from the repulsive nuclei. When localized at a vacancy in β -Ga₂O₃ the annihilation occurs mainly with valence electron states of the neighboring atoms. Both Ga 3d and O 2s/p states have a rather broad momentum distribution.
4. Electron-positron correlation effects.

The β -Ga₂O₃ structure has a low symmetry compared to many well-known systems with anisotropic positron signals such as Si in the diamond lattice structure. As noted above, the positron density distribution is rather anisotropic and runs along the tubes in the [010] direction. In Si the positrons also favor specific channels along the {110} directions (see Fig. 3c) but the intersecting tubes and the annihilating pair momentum density retain the cubic symmetry of the lattice. On the other hand, point defects in β -Ga₂O₃ occur only in specific orientations (see, for example, Fig. 7) and their anisotropic fingerprints do not average out to a more isotropic spectrum. This can be compared to, for example, a vacancy-donor pair in Si, which has 4 possible symmetric orientations occurring randomly in a real sample. In conclusion, for single crystals, in which the positron signal is not averaged between differently oriented grains, the anisotropy of the signal of any β -Ga₂O₃ sample naturally follows from the structure of the lattice and the simple point defects.

For a positron delocalized in the β -Ga₂O₃ lattice, we have analyzed the points 1 and 2 of the above list in detail. First of all, we have calculated the electron momentum density and the Compton profiles within the independent-particle model and impulse approximation in full consistence with our positron modeling. This is equivalent to setting the positron orbital to a constant and neglecting the enhancement factors in the model [32] we use for the momentum density of annihilating pairs. Second, we analyze the positron momentum density (the Fourier coefficients of the orbital) in order to understand if the anisotropy of the positron orbital alone could increase the anisotropy of the momentum density of annihilating pairs. The Compton profile lineshapes (S and W type parameters extracted from the profiles) turn out to reflect the same kind of anisotropy as the Doppler spectra in the β -Ga₂O₃ lattice, which implies that the lattice state anisotropy is an inherent property of the β -Ga₂O₃ electronic structure. According to the Fourier components of the positron orbital, the positron is "free"

along the [010] direction and confined in the perpendicular directions (see Fig. 3c), as in the perpendicular directions the positron momentum density displays a broadening. The anisotropic nature of the positron momentum density has a role in determining the full anisotropy, as the momentum density of annihilating pairs is approximately the electron momentum density convoluted with the positron momentum density. Also, the positron density gives a larger weight to the outermost valence orbitals of ions in the interstitial region of the lattice, where the electron-positron correlations have the strongest effects. Separating and quantifying the roles of these mechanisms is, however, difficult.

In the case of defects trapping the positron, the Doppler broadening measures the electron-momentum density at the annihilation site but the confinement of the positron might also play a role. We find that the shape of the positron density is correlated to the (S, W) parameters in β -Ga₂O₃ in an intriguing way. In the β -Ga₂O₃ lattice and defects, the overall highest S parameters (and typically the lowest W parameters) are found in the [010] lattice direction. This direction corresponds to the open structure and the least dense lattice planes (Fig. 2) and to the direction along which the tubular positron states are formed in the β -Ga₂O₃ lattice (Fig. 3). Interestingly, in the [100]-[001] plane the local extrema of the (S, W) parameters are not found in "high-symmetry" [100] and [001] lattice directions in all cases. This is particularly visible in $V_{\text{Ga}}^{\text{ib}}$ and $V_{\text{Ga}}^{\text{ic}}$ that are very similar defects: their structures differ mainly by a rotation of $\sim 105^\circ$ (Fig. 7) and their positron lifetimes are essentially the same (Table II). However, the directions of the local maxima and minima of the (S, W) parameters in the [100]-[001] lattice plane differ by $\sim 45^\circ$.

The directions of the local (S, W) parameter extrema in the [100]-[001] plane are correlated with the direction of the longitudinal axis of the the positron density in all defects where the positron density has a clearly non-spherical shape. The minima of the S parameter in the [100]-[001] plane are rotated by 90° from the in-plane S parameter maxima, and hence correlated with the "narrow axis" of the positron density. These correlations are best visible in $V_{\text{Ga}}^{\text{ib}}$ and $V_{\text{Ga}}^{\text{ic}}$, and in particular when adding a second hydrogen to $V_{\text{Ga}}^{\text{ib}}$. The maximum S parameter in the [100]-[001] plane in $V_{\text{Ga}}^{\text{ib}}$ and $V_{\text{Ga}}^{\text{ib}}\text{-1H}$ is in the [100] direction while the longitudinal axis of their positron densities point is aligned with the [100] lattice direction as well. The maximum S parameter of $V_{\text{Ga}}^{\text{ic}}$, $V_{\text{Ga}}^{\text{ic}}\text{-1H}$ and $V_{\text{Ga}}^{\text{ic}}\text{-2H}$ in the [100]-[001] plane is found rotated by 45° from [100] towards the [001] lattice vector, as does the longitudinal axes of their positron densities. Adding a second hydrogen to $V_{\text{Ga}}^{\text{ib}}\text{-2H}$ rotates the positron density by approximately 45° from the [100] lattice vector towards [001], parallel to positron densities in the $V_{\text{Ga}}^{\text{ic}}$ defects. The local (S, W) parameter extrema for $V_{\text{Ga}}^{\text{ib}}\text{-2H}$ are in the same directions as for $V_{\text{Ga}}^{\text{ic}}\text{-2H}$.

The correlation between the shape of the positron density and the Doppler broadening parameters is consistent

with the following mechanism. An elongated positron density in a certain direction indicates less localization in this spatial dimension. Less localization in real space goes hand-in-hand with a stronger localization in momentum space, that is a narrower momentum distribution. However, we point out that also the local ionic structure and its orientation plays a role. In any case, for localized positrons the overall anisotropy of the Doppler signals increases by a factor of up to 2-3 in the *ib* and *ic* type split Ga vacancies.

Another manifestation of large anisotropy in positron annihilation radiation of a reduced symmetry system is the case of graphite [49], in which the positron is confined in 2D states between the sheets and samples predominantly the p_z orbitals of the carbon atoms, giving rise to a similar bimodal structure in the momentum density of annihilating pairs and a strong anisotropic Doppler spectra. This comparison to graphite demonstrates that the colossal magnitude of the anisotropic features in the Doppler broadening in $\beta\text{-Ga}_2\text{O}_3$ is only colossal when compared to typical widely studied semiconductors such as Si, GaAs, GaN or ZnO with high-symmetry crystal structures. Two-dimensional and in the case of $\beta\text{-Ga}_2\text{O}_3$ one-dimensional positron states should perhaps be expected to produce anisotropic Doppler broadening signals, and the exact nature of the positron state in a given crystal structure can only be determined by performing advanced theoretical calculations. Finally, it should be noted that the strongly one-dimensional positron state in the $\beta\text{-Ga}_2\text{O}_3$ lattice suggests that positron diffusion might be significantly faster along the [010] lattice direction than in the other directions. This should be considered in detail in future experiments.

VII. SUMMARY

Inspired by the colossal anisotropy in the Doppler broadening parameters measured in $\beta\text{-Ga}_2\text{O}_3$, we present a comprehensive theoretical study of positron annihilation signals in the $\beta\text{-Ga}_2\text{O}_3$ lattice and the various Ga mono-vacancy defects that this lattice is able to host. We also performed systematic angle-resolved Doppler broadening experiments that confirm the findings obtained by the state-of-the-art calculations of the positron states and positron-electron annihilation parameters. We address the primary difficulty in studying defects with positron annihilation in $\beta\text{-Ga}_2\text{O}_3$, caused by a combination of (i) signal anisotropy of unprecedented magnitude for 3D crystals and (ii) relatively small differences between signals $\beta\text{-Ga}_2\text{O}_3$ lattice and the various types of Ga mono-vacancy defects. In essence, the positron signal anisotropy in $\beta\text{-Ga}_2\text{O}_3$ is larger than the difference between lattice and vacancy signals and the (S, W) parameters of $\beta\text{-Ga}_2\text{O}_3$ lattice and vacancies overlap strongly.

The unusual symmetry properties of the monoclinic $\beta\text{-Ga}_2\text{O}_3$ lattice are at the origin of the anisotropy and the defect identification difficulties in several ways. First,

the delocalized positron state in the $\beta\text{-Ga}_2\text{O}_3$ lattice is found to form one-dimensional tubes along the [010] lattice direction, in contrast to three-dimensionally delocalized positron states in more typical crystal structures with cubic or hexagonal symmetry. This leads to 5-10-fold differences of the (S, W) parameters measured along different lattice directions compared to those found in, for example, Si or ZnO. Second, energetically favorable configurations of Ga mono-vacancies involve strong relaxations leading to highly non-symmetric split Ga vacancy configurations [6, 7, 9, 10]. The localized positron state is highly non-spherical (anisotropic) in these defects, further increasing the magnitude of the anisotropy by a factor of up to 3, in contrast to the typical mono-vacancy defects in other semiconductor crystals which exhibit at most the same barely noticeable magnitude of anisotropy as the lattice. Finally, the particularly low formation enthalpies [6, 7] of all of the Ga mono-vacancy defects in $\beta\text{-Ga}_2\text{O}_3$ lead to the situation where all samples appear to contain high concentrations ($>1 \times 10^{18} \text{ cm}^{-3}$) of split Ga vacancies. This causes difficulties for positron annihilation spectroscopies that are strongly comparative in nature and require a well-defined reference samples, preferably one that does not show positron trapping at any vacancy type defects, for detailed defect identification.

In spite of all the difficulties in interpreting positron annihilation data caused by the colossal anisotropy of the Doppler broadening parameters, there is a possibility of taking advantage of the phenomenon. We suggest that positron states can be differentiated by the differences in the nature of the signal anisotropy. This can be achieved by performing experiments in more than one directions and analyzing the shape of the Doppler broadening by using multiple integration windows for the S and W parameters. Importantly, the signal anisotropy must be taken into account when performing Doppler broadening experiments in $\beta\text{-Ga}_2\text{O}_3$, and the measurement direction in relation to the crystal orientation needs to be analyzed in detail when presenting experimental data. In future work on positron annihilation in $\beta\text{-Ga}_2\text{O}_3$, it is imperative to pay close attention to the measurement directions and give detailed account of the measurement geometry.

ACKNOWLEDGMENTS

We wish to thank Mr. Vitomir Sever and Ms. Daria Kriukova for technical assistance in the angle-resolved Doppler experiments. We acknowledge the computational resources provided by CSC (Finnish IT Centre for Science). This work was partially supported by the Academy of Finland grants Nr 285809, 315082 and 319178. A. Karjalainen wishes to thank the Magnus Ehrnrooth foundation for financial support. This work was partially performed under the auspices of the U.S. DOE by Lawrence Livermore National Laboratory under contract DE-AC52-07NA27344, and supported by the

[1] S. Pearton, J. Yang, P. H. Cary IV, F. Ren, J. Kim, M. J. Tadjer, and M. A. Mastro, A review of Ga_2O_3 materials, processing, and devices, *Appl. Phys. Rev.* **5**, 011301 (2018).

[2] M. Higashiwaki, H. Murakami, Y. Kumagai, and A. Kurokawa, Current status of Ga_2O_3 power devices, *Jpn. J. Appl. Phys.* **55**, 1202A1 (2016).

[3] M. D. McCluskey, Point defects in Ga_2O_3 , *J. Appl. Phys.* **127**, 101101 (2020).

[4] P. Jiang, X. Qian, X. Li, and R. Yang, Three-dimensional anisotropic thermal conductivity tensor of single crystalline β - Ga_2O_3 , *Appl. Phys. Lett.* **113**, 232105 (2018).

[5] N. Ueda, H. Hosono, R. Waseda, and H. Kawazoe, Anisotropy of electrical and optical properties in β - Ga_2O_3 single crystals, *Appl. Phys. Lett.* **71**, 933 (1997).

[6] J. B. Varley, H. Peelaers, A. Janotti, and C. G. Van de Walle, Hydrogenated cation vacancies in semiconducting oxides, *J. Phys.: Condens. Matter* **23**, 334212 (2011).

[7] M. Ingebrigtsen, A. Y. Kuznetsov, B. Svensson, G. Alfieri, A. Mihaila, U. Badstübler, A. Perron, L. Vines, and J. Varley, Impact of proton irradiation on conductivity and deep level defects in β - Ga_2O_3 , *APL Mater.* **7**, 022510 (2019).

[8] S. Lany, Defect phase diagram for doping of Ga_2O_3 , *APL Mater.* **6**, 046103 (2018).

[9] P. Weiser, M. Stavola, W. B. Fowler, Y. Qin, and S. Pearton, Structure and vibrational properties of the dominant OH center in β - Ga_2O_3 , *Appl. Phys. Lett.* **112**, 232104 (2018).

[10] J. M. Johnson, Z. Chen, J. B. Varley, C. M. Jackson, E. Farzana, Z. Zhang, A. R. Arehart, H.-L. Huang, A. Genc, S. A. Ringel, C. G. Van de Walle, D. A. Muller, and J. Hwang, Unusual formation of point-defect complexes in the ultrawide-band-gap semiconductor β - Ga_2O_3 , *Phys. Rev. X* **9**, 041027 (2019).

[11] F. Tuomisto and I. Makkonen, Defect identification in semiconductors with positron annihilation: Experiment and theory, *Rev. Mod. Phys.* **85**, 1583 (2013).

[12] K. Saarinen, T. Laine, S. Kuisma, J. Nissilä, P. Hau-tojärvi, L. Dobrzynski, J. M. Baranowski, K. Pakula, R. Stepniewski, M. Wojdak, A. Wysmolek, T. Suski, M. Leszczynski, I. Grzegory, and S. Porowski, Observation of native Ga vacancies in GaN by positron annihilation, *Phys. Rev. Lett.* **79**, 3030 (1997).

[13] F. Tuomisto, V. Ranki, K. Saarinen, and D. C. Look, Evidence of the Zn vacancy acting as the dominant acceptor in *n*-type ZnO, *Phys. Rev. Lett.* **91**, 205502 (2003).

[14] J.-M. Mäki, I. Makkonen, F. Tuomisto, A. Karjalainen, S. Suihkonen, J. Räisänen, T. Y. Chemekova, and Y. N. Makarov, Identification of the $\text{V}_{\text{Al}}\text{-O}_n$ defect complex in AlN single crystals, *Phys. Rev. B* **84**, 081204 (2011).

[15] C. Rauch, I. Makkonen, and F. Tuomisto, Identifying vacancy complexes in compound semiconductors with positron annihilation spectroscopy: A case study of InN, *Phys. Rev. B* **84**, 125201 (2011).

[16] E. Korhonen, F. Tuomisto, O. Bierwagen, J. S. Speck, and Z. Galazka, Compensating vacancy defects in Sn- and Mg-doped In_2O_3 , *Phys. Rev. B* **90**, 245307 (2014).

[17] S. F. Chichibu, A. Uedono, T. Onuma, B. A. Haskell, A. Chakraborty, T. Koyama, P. T. Fini, S. Keller, S. P. DenBaars, J. S. Speck, U. K. Mishra, S. Nakamura, S. Yamaguchi, S. Kamiyama, H. Amano, I. Akasaki, J. Han, and T. Sota, Origin of defect-insensitive emission probability in In-containing (Al,In,Ga)N alloy semiconductors, *Nature Mater.* **5**, 810 (2006).

[18] A. Uedono, K. Tenjinbayashi, T. Tsutsui, Y. Shimahara, H. Miyake, K. Hiramatsu, N. Oshima, R. Suzuki, and S. Ishibashi, Native cation vacancies in Si-doped AlGaN studied by monoenergetic positron beams, *J. Appl. Phys.* **111**, 013512 (2012).

[19] V. Prozheeva, I. Makkonen, R. Cusco, L. Artus, A. Dadgar, F. Plazaola, and F. Tuomisto, Radiation-induced alloy rearrangement in $\text{In}_x\text{Ga}_{1-x}\text{N}$, *Appl. Phys. Lett.* **110**, 132104 (2017).

[20] A. Uedono, T. Nabatame, W. Egger, T. Koschine, C. Hugenschmidt, M. Dickmann, M. Sumiya, and S. Ishibashi, Vacancy-type defects in $\text{Al}_2\text{O}_3/\text{GaN}$ structure probed by monoenergetic positron beams, *J. Appl. Phys.* **123**, 155302 (2018).

[21] S. Ishibashi, A. Uedono, H. Kino, T. Miyake, and K. Terakura, Computational study of positron annihilation parameters for cation mono-vacancies and vacancy complexes in nitride semiconductor alloys, *J. Phys.: Condens. Matter* **31**, 475401 (2019).

[22] V. Prozheeva, I. Makkonen, H. Li, S. Keller, U. K. Mishra, and F. Tuomisto, Interfacial N vacancies in GaN/(Al,Ga)N/GaN heterostructures, *Phys. Rev. Applied* **13**, 044034 (2020).

[23] W.-Y. Ting, A. H. Kitai, and P. Mascher, Crystallization phenomena in β - Ga_2O_3 investigated by positron annihilation spectroscopy and X-ray diffraction analysis, *Mater. Sci. Eng. B* **91-92**, 541 (2002).

[24] E. Korhonen, F. Tuomisto, D. Gogova, G. Wagner, M. Baldini, Z. Galazka, R. Schewski, and M. Albrecht, Electrical compensation by Ga vacancies in Ga_2O_3 thin films, *Appl. Phys. Lett.* **106**, 242103 (2015).

[25] F. Tuomisto, A. Karjalainen, V. Prozheeva, I. Makkonen, G. Wagner, and M. Baldini, Ga vacancies and electrical compensation in β - Ga_2O_3 thin films studied with positron annihilation spectroscopy, in *Oxide-based Materials and Devices X*, Vol. 10919 (International Society for Optics and Photonics, 2019) p. 1091910.

[26] G. Kresse and J. Furthmüller, Efficient iterative schemes for ab initio total-energy calculations using a plane-wave basis set, *Phys. Rev. B* **54**, 11169 (1996).

[27] G. Kresse and J. Furthmüller, Efficiency of ab-initio total energy calculations for metals and semiconductors using a plane-wave basis set, *Comput. Mater. Sci.* **6**, 15 (1996).

[28] G. Kresse and D. Joubert, From ultrasoft pseudopotentials to the projector augmented-wave method, *Phys. Rev. B* **59**, 1758 (1999).

[29] P. E. Blöchl, Projector augmented-wave method, *Phys.*

Rev. B **50**, 17953 (1994).

[30] E. Boroński and R. M. Nieminen, Electron-positron density-functional theory, Phys. Rev. B **34**, 3820 (1986).

[31] M. J. Puska, A. P. Seitsonen, and R. M. Nieminen, Electron-positron Car-Parrinello methods: Self-consistent treatment of charge densities and ionic relaxations, Phys. Rev. B **52**, 10947 (1995).

[32] M. Alatalo, B. Barbiellini, M. Hakala, H. Kauppinen, T. Korhonen, M. J. Puska, K. Saarinen, P. Hautajärvi, and R. M. Nieminen, Theoretical and experimental study of positron annihilation with core electrons in solids, Phys. Rev. B **54**, 2397 (1996).

[33] I. Makkonen, M. Hakala, and M. J. Puska, Calculation of valence electron momentum densities using the projector augmented-wave method, J. Phys. Chem. Solids **66**, 1128 (2005); Modeling the momentum distributions of annihilating electron-positron pairs in solids, Phys. Rev. B **73**, 035103 (2006).

[34] M. Matsumoto, M. Tokii, and S. Wakoh, An improvement of the linear tetrahedron method for compton profile calculations, J. Phys. Soc. Jpn. **73**, 1870 (2004).

[35] K. Momma and F. Izumi, *VESTA3* for three-dimensional visualization of crystal, volumetric and morphology data, J. Appl. Crystallogr. **44**, 1272 (2011).

[36] W. Humphrey, A. Dalke, and K. Schulter, VMD – Visual Molecular Dynamics, J. Mol. Graph. **14**, 33 (1996).

[37] J. Stone, *An Efficient Library for Parallel Ray Tracing and A[5]hakoniM. Johansen, A. Zubiaga, I. Makkonen, F. Tuomisto, P. T. Neuvonen, K. E. Knutson, E. V. Monakhov, A. Y. Kuznetsov, and B. G. Svensson, Identification of substitutional Li in *n*-type ZnO and its role as an acceptor, Phys. Rev. B **83**, 245208 (2011).*

[38] I. Kanazawa, S. Tanigawa, R. Suzuki, Y. Mizuhara, M. Sano, and H. Inokuchi, Two-dimensional electron momentum distribution in graphite revealed by means of angular correlation of positron annihilation, J. Phys. Chem. Solids **48**, 701 (1987).

[39] L. Yongming, B. Johansson, and R. M. Nieminen, Two-dimensional electron momentum distribution of graphite, J. Phys.: Condens. Matter **3**, 1699 (1991).

[40] S. Ishibashi, Calculation of positron states in carbon-nanotube bundles, J. Phys.: Condens. Matter **14**, 9753 (2002).

[41] F. Linez, I. Makkonen, and F. Tuomisto, Calculation of positron annihilation characteristics of six main defects in 6H-SiC and the possibility to distinguish them experimentally, Phys. Rev. B **94**, 014103 (2016).

[42] S. Dannefaer, W. Puff, and D. Kerr, Positron line-shape parameters and lifetimes for semiconductors: Systematics and temperature effects, Phys. Rev. B **55**, 2182 (1997).

[43] A. Zubiaga, F. Tuomisto, J. Zuñiga-Pérez, and V. Muñoz-San José, Characterization of non-polar ZnO layers with positron annihilation spectroscopy, Acta Phys. Pol. A **114**, 1457 (2008).

[44] I. Makkonen, E. Korhonen, V. Prozheeva, and F. Tuomisto, Identification of vacancy defect complexes in transparent semiconducting oxides ZnO, In₂O₃ and SnO₂, J. Phys.: Condens. Matter **28**, 224002 (2016).

[45] M. Hakala, M. J. Puska, and R. M. Nieminen, Momentum distributions of electron-positron pairs annihilating at vacancy clusters in Si, Phys. Rev. B **57**, 7621 (1998).

[46] Z. Galazka, K. Irmscher, R. Uecker, R. Bertram, M. Pietsch, A. Kwasniewski, M. Naumann, T. Schulz, R. Schewski, D. Klimm, and M. Bickermann, On the bulk β -Ga₂O₃ single crystals grown by the Czochralski method, J. Crystal Growth **404**, 184 (2014).

[47] J. Åhman, G. Svensson, and J. Albertsson, A Reinvestigation of β -Gallium Oxide, Acta Crystallogr. C **52**, 1336 (1996).

[48] J. B. Varley, First-principles calculations 2 - doping and defects in Ga₂O₃, in *Gallium Oxide - Materials Properties, Crystal Growth, and Devices*, edited by M. Higashiwaki and S. Fujita (Springer, 2020) p. 329.

[49] Z. Tang, M. Hasegawa, Y. Nagai, M. Saito, and Y. Kawazoe, First-principles calculation of coincidence Doppler broadening of positron annihilation radiation, Phys. Rev. B **65**, 045108 (2002).

[50] S. Hautakangas, I. Makkonen, V. Ranki, M. J. Puska, K. Saarinen, X. Xu, and D. C. Look, Direct evidence of impurity decoration of Ga vacancies in GaN from positron annihilation spectroscopy, Phys. Rev. B **73**, 193301 (2006).

[51] F. Tuomisto, V. Prozheeva, I. Makkonen, T. H. Myers, M. Bockowski, and H. Teisseire, Amphoteric Be in GaN: Experimental evidence for switching between substitutional and interstitial lattice sites, Phys. Rev. Lett. **119**, 196404 (2017).

[52] A. Zubiaga, F. Tuomisto, V. A. Coleman, H. H. Tan, C. Jagadish, K. Koike, S. Sasa, M. Inoue, and M. Yano, Mechanisms of electrical isolation in O⁺-irradiated ZnO, Phys. Rev. B **78**, 035125 (2008).

*

Appendix A

Anticipating the emergence of an experimentally well-defined reference $\beta\text{-Ga}_2\text{O}_3$ sample, we show for the benefit of future work the defect-lattice ratio curves for all the defects considered in this work in Figs. 14, 15 and 16. The ratio curves are normalized by the lattice Doppler spectrum in each of the three directions ([001], [010] and [100]). Interestingly, the ratio curves in the [001] direction (for all defects) appear the most ordinary in the sense that their shapes remind those obtained for various types of defects in GaN [50, 51] and ZnO [52, 53]. In this direction, the shoulder-like feature around 1.5 a.u. is the least pronounced for most of the defects. Note that this shoulder-like feature, that in some cases resembles a peak, is typical of metal-oxide lattices where the atomic fraction of oxygen is higher than 50 % [44]. The origin of this shoulder is in the strong contribution from O 2p electrons in this momentum range. At higher momenta, Ga 3d electrons dominate the annihilations. The strength of this feature could in principle be used to distinguish between the different defects in measurements performed in a given direction, in particular in cases where maximum value of the ratio switches from below 1 to above 1 (for example, regular mono-vacancy vs. split Ga vacancy). In practice, however, the reliability of this identification criterion is hard to assess as this is the momentum range where the functional shape of the Doppler spectrum changes from Gaussian to (sub-)exponential and the detector resolution plays a significant role [41]. Comparing the differences in the anisotropic behavior of the defects remains more reliable an approach in $\beta\text{-Ga}_2\text{O}_3$.

The shoulder/peak feature at around 1.5 a.u. is at the origin of the S parameter decreasing below that of the $\beta\text{-Ga}_2\text{O}_3$ lattice for some of the defects. In addition, it dominates the signal intensity of the W parameter region as seen from the grey shaded areas in Figs. 14, 15 and 16. This suggests that the difficulties with the overlap of the lattice and vacancy signals could be mitigated to some extent by modifying the (S, W) parameter integration windows for improved differentiation, at the expense of statistical accuracy. In the following, we consider alternative (S, W) parameter integration windows shown with the dotted lines in the ratio curve plots. The windows are changed from [0, 0.45] a.u. to [0, 0.40] a.u. for the S parameter and the lower limit of the W windows is shifted from 1.54 a.u. to 2.0 a.u. The upper limit of W parameter was not changed as the momentum distribution intensity is almost negligible already at 4 a.u.

Fig. 17 shows the (S, W) parameters analyzed with the alternative windows, normalized to $\beta\text{-Ga}_2\text{O}_3$ lattice in the [001] lattice direction. The effect of changing the S parameter window on the relative S parameters is minimal. The removal of the shoulder effect from the W parameter decreases the W parameter of vacancy defects and improves the overlap situation, but not dramatically. With the W parameter windows starting from 2.00 a.u., the $\beta\text{-Ga}_2\text{O}_3$ lattice produces the highest W parameter in the [100] and [010] lattice directions, providing additional means to distinguish between the lattice and defects. However, this narrowed W parameter window reduces the statistical weight of the W parameter by a factor of 3 to only about 2 % of the whole 511-keV annihilation peak, making analysis less accurate. Generally, changes in the S parameter are more reliably monitored. Nevertheless, the future process of identifying a "defect-free" reference $\beta\text{-Ga}_2\text{O}_3$ sample will benefit from examining alternative W parameter windows to differentiate between defect and lattice signals.

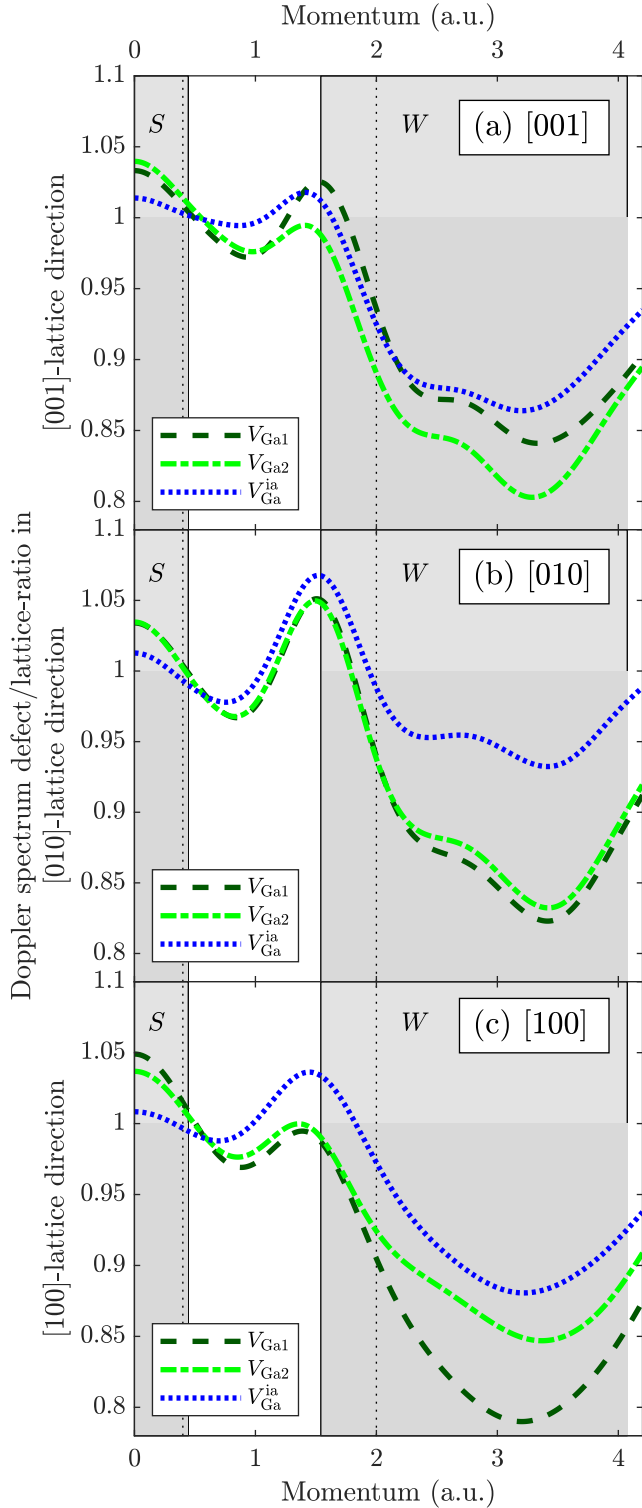


FIG. 14: Vacancy/lattice-ratios of defects $V_{\text{Ga}1}$, $V_{\text{Ga}2}$ and $V_{\text{Ga}}^{\text{ia}}$.

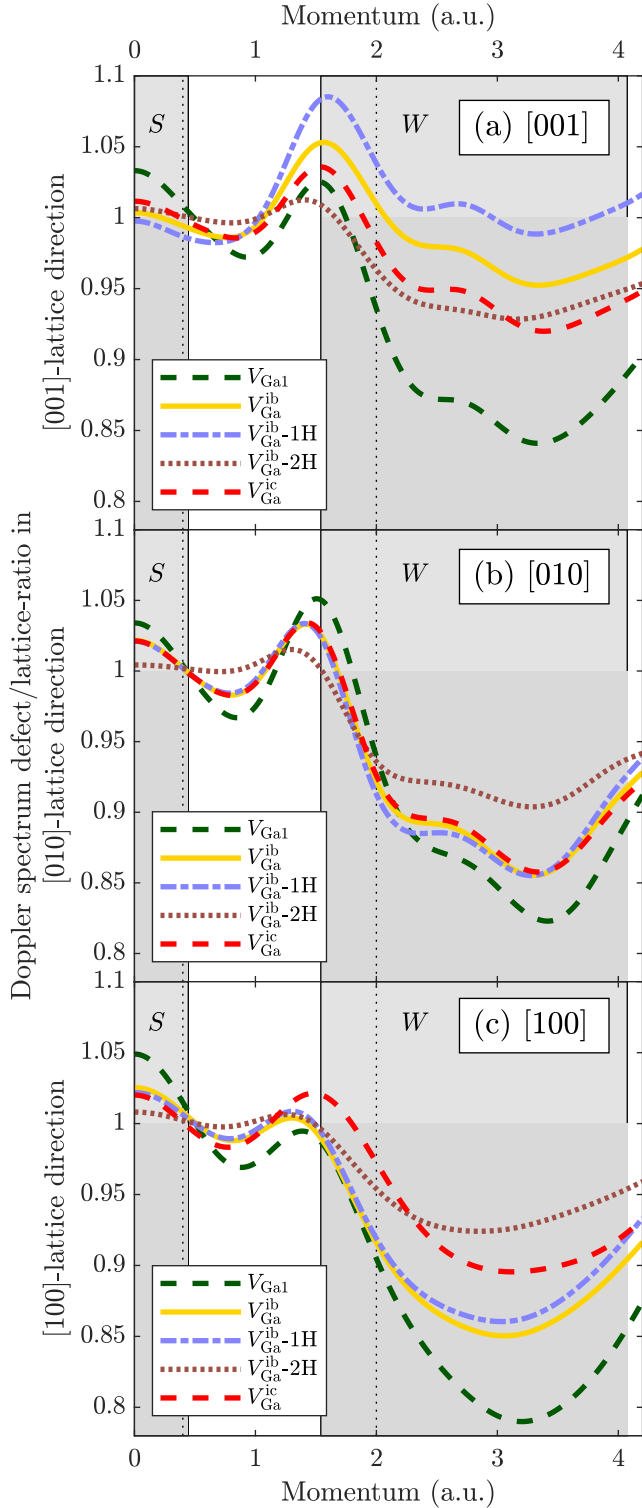


FIG. 15: Vacancy/lattice-ratios of defects $V_{\text{Ga}1}$, $V_{\text{Ga}}^{\text{ib}}$, $V_{\text{Ga}}^{\text{ib}}-1\text{H}$, $V_{\text{Ga}}^{\text{ib}}-2\text{H}$ and $V_{\text{Ga}}^{\text{ic}}$.

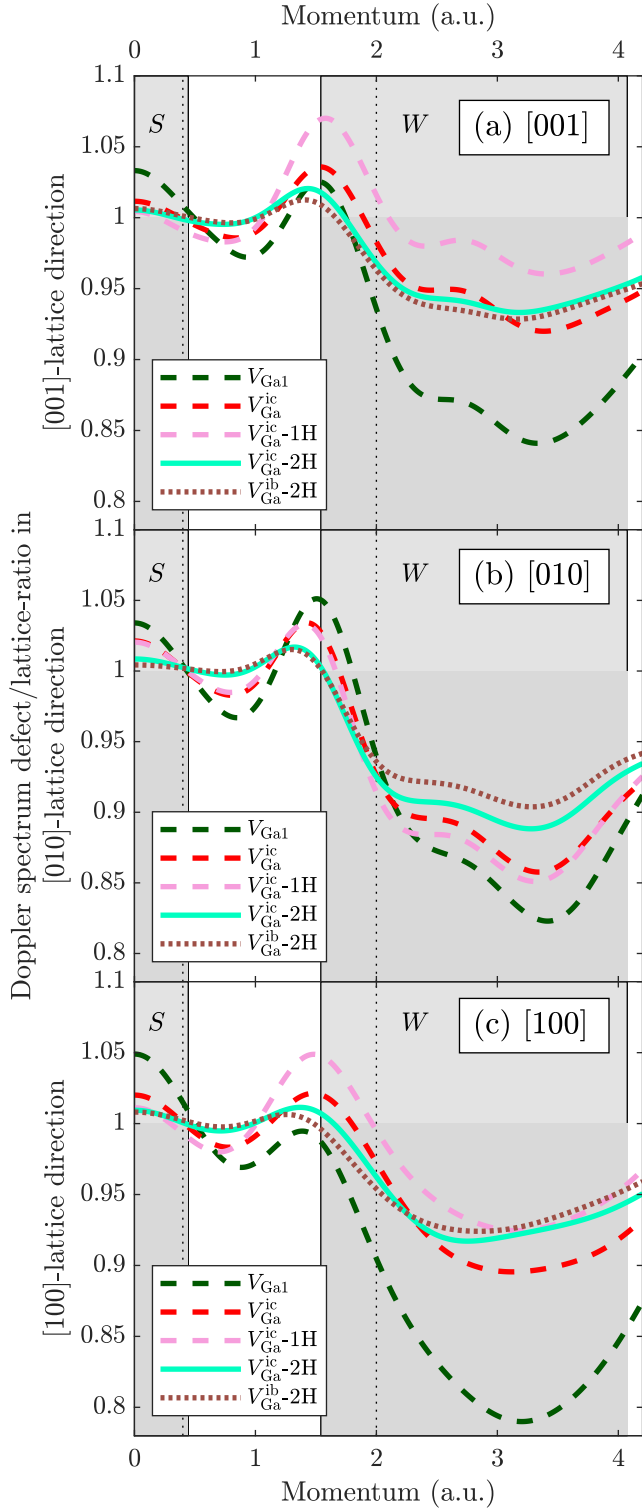


FIG. 16: Vacancy/lattice-ratios of defects $V_{\text{Ga}1}$, $V_{\text{Ga}}^{\text{ic}}$, $V_{\text{Ga}}^{\text{ic}}\text{-1H}$, $V_{\text{Ga}}^{\text{ic}}\text{-2H}$ and $V_{\text{Ga}}^{\text{ib}}\text{-2H}$.

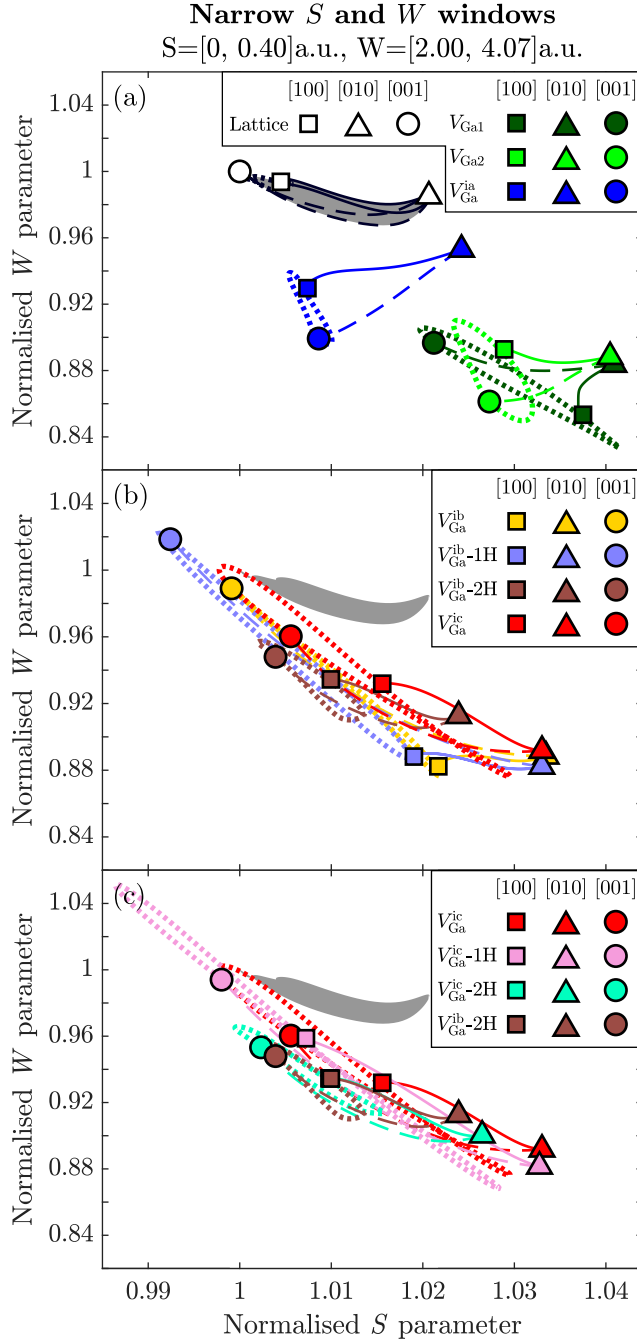


FIG. 17: The (S, W) parameters of the lattice and vacancies calculated with alternative (S, W) parameter windows. The (S, W) parameters are normalized to the $\beta\text{-Ga}_2\text{O}_3$ lattice in the $[001]$ lattice direction. The grey shadow illustrates the (S, W) parameter of the $\beta\text{-Ga}_2\text{O}_3$ lattice. The figure uses the notation introduced in Fig. 5.